J. Fluid Mech. (2001), *vol.* 427, *pp.* 1–28. Printed in the United Kingdom

Streamwise oscillations of a cylinder in a steady current. Part 1. Locked-on states of vortex formation and loading

By O. CETINER† AND D. ROCKWELL

Department of Mechanical Engineering and Mechanics, 354 Packard Laboratory, 19 Memorial Drive West, Lehigh University, Bethlehem, PA 18015

(Received 22 April 1999 and in revised form 24 July 2000)

Streamwise oscillations of a circular cylinder in a steady uniform flow are investigated experimentally using a technique of high-image-density particle image velocimetry, in conjunction with instantaneous force measurements. This approach allows insight into the relationship between the loading and the patterns of vorticity and streamline topology in the near wake.

In analogy with the classical locked-on state arising from transverse oscillations of a cylinder in uniform flow, it is possible to attain either locked-on or quasi-locked-on states due to streamwise oscillations. In these cases, however, the repetitive signature of the transverse force is not sinusoidal; rather, it is strongly modulated and the corresponding spectra can exhibit several sharply defined peaks. The predominant peak can vary over a remarkably wide range, extending from the subharmonic to the third harmonic of the cylinder oscillation frequency; for certain locked-on states of the transverse force signature, the spectral peak at the cylinder oscillation frequency is actually suppressed. Corresponding instantaneous traces and spectra of the in-line force simply show dominance of the spectral peak at the cylinder oscillation frequency. Further interpretation of the loading is provided in terms of Lissajous patterns of the transverse and in-line force coefficients.

All of these features are related to the instantaneous patterns of vortex formation in the near wake. During a typical cycle of the cylinder oscillation, these patterns can be divided into two broad categories: Kármán-like shedding; and a nearly 'frozen' array of shed vortices. The order of occurrence of these basic patterns during an oscillation cycle dictates the instantaneous signatures and time-averaged spectra of the transverse force.

1. Introduction

Long-wave motion past a cylinder, both without and with a steady current, has been recognized for some time as an important origin of unsteady loading. The limiting case of infinitely long wavelength can be effectively simulated by either unidirectional, oscillatory flow past a stationary cylinder or unidirectional oscillations of a cylinder in quiescent fluid. To simulate the effects of current, a steady component of flow, or steady motion of the cylinder, is superposed on the oscillatory component.

In-line oscillations of a cylinder in a steady, uniform flow are distinctly different from the celebrated case of transverse oscillations; the insight gained into the latter

† Present address: Istanbul Technical University, Turkey.

category will, however, provide a valuable framework for interpreting corresponding in-line oscillations. Perhaps the most visible consequence of transverse oscillations is the occurrence of locked-on vortex formation, which has been assessed by Sarpkaya (1979), Bearman (1984), Rockwell (1990), Griffin & Hall (1991, 1995) and Hall & Griffin (1993). The major focus of the wide variety of experimental investigations that have pursued insight into the structure of the near wake has been qualitative visualization of the overall vortex patterns, with the aim of determining the origin of loading of the cylinder. Zdravkovich (1982), Öngoeren & Rockwell (1988) and Williamson & Roshko (1988) related alterations in the patterns of vortex formation to changes in both the magnitude and phase of the fluctuating lift. Recently, the patterns of near-wake vortices have been assessed by quantitative imaging techniques, which provide instantaneous vorticity distributions and streamline topology. Rockwell *et al.* (1993) provide images of the quasi-two-dimensional and three-dimensional near wake. Gu, Chyu & Rockwell (1994) and Sheridan *et al.* (1998) employ similar approaches, with emphasis on description of the timing of quasi-two-dimensional vortex formation from an oscillating cylinder. Related investigations employing numerical simulations include those of Lu & Dalton (1996) and Blackburn & Henderson (1995, 1999), both of which showed changes in the timing of the initially shed concentration of vorticity, which is in accord with the observation with the results of Gu *et al.* (1994).

Also relevant to the present case of in-line oscillations of a cylinder in steady flow is the limiting scenario of oscillations in the absence of a steady current. The patterns of vortex formation and the associated in-line and transverse force components exhibit a rich variety of possibilities over the range of Keulegan–Carpenter number $KC = 2\pi A/D$ of practical interest, in which A represents the amplitude of oscillation of a cylinder of diameter D. Investigations and overviews of these features are provided by Singh (1979), Bearman *et al.* (1981), Sarpkaya & Isaacson (1981), Ikeda & Yamamoto (1981), Iwagaka, Asano & Nagai (1983), Williamson (1985), Obasaju, Bearman & Graham (1988), and Lin & Rockwell (1999). Related numerical simulations are summarized in the works of Sarpkaya (1989), Lin, Bearman & Graham (1996) and Lin & Rockwell (1999).

When in-line, small-amplitude oscillation of a cylinder occurs in a steady uniform flow, possible patterns of vortex formation include those revealed by Griffin & Ramberg (1976). They focused on the onset of locked-on patterns of vortex formation at relatively low amplitudes of the cylinder motion. Öngoeren & Rockwell (1988) defined patterns of vortex formation over a wider range of excitation frequency and found, in addition to the vortex patterns of Griffin & Ramberg (1976), combinations of counter-rotating vortex pairs and single vortices. Numerical solution of the Navier–Stokes equations was employed by Lecointe & Piquet (1989) to verify the existence of selected modes of Öngoeren & Rockwell (1988). The foregoing characterizations of the wake vortex patterns complement studies of the unsteady loading on a cylinder oscillating in the in-line direction at small amplitude, addressed experimentally by Tanida, Okajima & Watanabe (1973) and numerically by Hurlbut, Spaulding & White (1982).

The intermediate wake region of cylinders undergoing in-line oscillations in the presence of steady flow can exhibit remarkable and complex patterns of vortices, as demonstrated by the calculations of Sarpkaya *et al.* (1992). Their study revealed, at sufficiently large amplitude of oscillation, a three-row vortex street, in addition to other patterns. In a similar spirit, Graham, Arkel & Zhou (1993) demonstrated interesting patterns of vortices in the intermediate wake region and, correspondingly, ordered modulation of the transverse force coefficient.

Sarpkaya & Storm (1985) measured the in-line force coefficients on a cylinder translating in oscillatory flow and accounted for both the Keulegan–Carpenter number KC and the ratio of the cylinder velocity to the current velocity. Verley & Moe (1979) undertook extensive qualitative flow visualization for a relatively wide range of these parameters. Based on this visualization, Zdravkovich (1996) suggested that if the conventional Keulegan–Carpenter number is replaced by a modified version due to Sarpkaya, Bakinis & Storm (1984), the regimes of vortex patterns can be described in a more orderly fashion.

The foregoing investigations have provided valuable information on a variety of complex features of vortex patterns and unsteady loading due to the simultaneous presence of both oscillating and mean components of either the fluid or cylinder motion. To date, quantitative patterns of the near-wake structure, e.g. instantaneous patterns of vorticity, have not been directly related to the corresponding instantaneous traces and spectra of the in-line and transverse forces; rather, experimental emphasis has been on either qualitative visualization of vortex patterns or measurement of forces. Moreover, the possible occurrence of new types of locked-on states of vortex formation at larger amplitudes, and over a range of oscillation frequencies, has not been addressed. If locked-on, highly repetitive states of vortex formation are indeed attainable, the issue arises as to whether the instantaneous traces of force fluctuations, especially those of the transverse force, exhibit generic forms that can be explained on the basis of instantaneous patterns of vorticity. If so, these generic types of force traces can be linked to fundamental types of spectra of the force fluctuations. The manner in which the predominant spectral components shift from low to high frequencies, or conversely, in relation to the form of the instantaneous force trace and the type of instantaneous vorticity field is unclarified. This underlying physics is central to gaining an understanding of the in-line oscillations of a cylinder in a steady current which, of course, represents the combined effect of steady current and unidirectional wave motion past a stationary cylinder.

In order to address these issues, the present study employs simultaneous techniques of high-image-density particle image velocimetry and in-line and transverse force measurements, leading to instantaneous links between patterns of vorticity and the induced forces on the cylinder.

The principal findings in this investigation start in § 3 with a discussion of time-averaged spectra of the forces. Then, with the aid of these spectra, which define the predominant spectral peaks, it is possible to address, in § 4, the form of the instantaneous force traces. These features of the unsteady loading serve as a prelude to § 5, which defines the basic modes of vortex patterns in the near wake that are associated with the forces. Then, § 6 characterizes the spectra and instantaneous force traces for wider ranges of parameters. Section 7 gives the concluding remarks and assesses the most critical findings.

2. Experimental system and techniques

Experiments were undertaken in a custom-designed, large-scale water channel that allows quantitative imaging. The main test section has a depth of 610 mm, a width of 914 mm and a length of 4928 mm. The water depth was maintained at 543 mm. This main test section is preceded by a 2 : 1 contraction with appropriate arrangements of honeycomb and screens to yield a turbulence intensity less than 0.1%. The range of flow velocities considered was $0 \leqslant U \leqslant 95\,\mathrm{mm\,s^{-1}}$, corresponding to values of Reynolds number $405 \leqslant Re \leqslant 2482$.

The experimental apparatus consisted of a cylinder of diameter 25.4 mm and length 318 mm. It was mounted in a horizontal, cantilevered arrangement at a location midway between the free surface and the bottom of the water channel. A small section of the cylinder 9.5 mm long and located a distance of 89 mm from the end was replaced by a thin-walled transparent cylinder, whose interior was filled with distilled water. This window minimized shadow effects arising from refractive distortion of the laser sheet that was generated during acquisition of PIV images.

The cylinder was mounted on a strain gauge sting in order to measure the unsteady in-line and transverse forces. The resonant frequency of the cylinder system was determined to be approximately 20 Hz, which is a factor of 24 times higher than the highest frequency of interest in this investigation. Circular endplates of 368 mm diameter and 6.4 mm thickness were located at each end of the cylinder. These plates had a 30° outward bevel. In order to ensure that the proximity of the endplates did not interfere with the measured force, a gap of 1 mm was maintained between the end of the cylinder and the near endplate, while a specially designed opening in the far endplate precluded contact with the strain gauge sting. Both axes of the strain gauge system were calibrated statically using a series of known weights suspended from the end of the cylinder. The accuracy of this calibration is estimated to be 0.7%. Further checks were employed to ensure that the strain gauge accurately measured the fluid force.

Another check involved the oscillatory flow (in the absence of steady current U) experiments of Obasaju *et al.* (1988). The peak values and relative phase shifts of both the in-line and transverse coefficients C_x and C_y of the present study at $KC = 6$ (not shown) were found to be close to theirs at $KC = 6.75$. First of all, the cylinder was oscillated in still fluid at values of $KC = 2\pi A/D = 1$, 2, and 10, where A is the oscillation amplitude and D is the cylinder diameter. The r.m.s. values of the in-line force coefficient $(C_x)_{rms}$ were compared with the theoretical values of Bearman *et al.* (1985); this procedure was repeated for both axes. The transverse C_y and horizontal C_x force coefficients are defined as $C = F/\frac{1}{2}\rho U_0^2 LD$, in which U_0 is the peak value of the cylinder velocity U_c at a reference Keulegan–Carpenter number $KC = 2\pi A/D = 6.0$. The corresponding value in terms of the steady free-stream velocity U is $C^* = F/\frac{1}{2}\rho U^2 LD$. The value of U was determined experimentally using both PIV and floating marker techniques; the uncertainty of U is estimated to be 0.5%.

This entire system of the cylinder and two endplates underwent controlled motion in the horizontal direction. A high-resolution computer-controlled stepping motor, controlled by the central microcomputer system, allowed precise control of the frequency and amplitude of the cylinder motion. In the first part of this investigation, emphasis is on the amplitude A of the cylinder oscillation for which the onset of pronounced antisymmetrical vortex shedding occurs in the absence of steady flow; it is represented by the Keulegan–Carpenter number $KC = 2\pi A/D = 6$. The frequency of oscillation of the cylinder was maintained at $f_e = 0.28$ Hz, corresponding to the frequency parameter $\beta = f_e D^2/\nu = 184$. At $KC = 6$, this value of β corresponds to an effective Reynolds number of the oscillatory component of the flow $(KC)(\beta) = 1104$. Variations in the free-stream velocity U yielded changes of the dimensionless frequency f_e/f_0, where f_0 is the Kármán shedding frequency from the corresponding stationary cylinder. The corresponding range of Reynolds number was $405 \leqslant Re \leqslant 2482$. Velocity U was measured independently. The value of f_0 was deduced from $f_0 D/U = 0.2$. Over the range, previous data indicate that $f_0 D/U = 0.2 \pm 0.015$; so $f_0 D/U = 0.2$ is a reasonable approximation for our purposes, where a reference value of f_0 is required. The relationship between the measured velocity U, f_e and f_0 can be written

as $U = f_e/D/(0.2f_e/f_0)$. Of course, variations in U induce changes in not only f_0, but also in normalized velocity $U/(2\pi f_e A)$ when f_e and A (or $KC = 2\pi A/D$) are maintained constant. The parameter $U/2\pi f_e A$ is therefore specified. We note, however, that it appears to have a weaker influence than frequency ratio f_e/f_0 on the occurrence of locked-on vortex formation and force variations, which are principal features of the present investigation. Unless otherwise noted, the foregoing conditions were employed for the results given in figures 1–9. In the second part of this study, the effect of changes in the Keulegan–Carpenter number were addressed for $1 \leqslant KC \leqslant 10$. Figures 10 to 12 exhibit the corresponding results.

Quantitative space–time imaging of the velocity and vorticity fields, as well as the corresponding streamline topology, was achieved using a laser scanning version of high-image-density particle image velocimetry (PIV), which was employed in a cine mode. This imaging was undertaken simultaneously with measurements of the instantaneous in-line and transverse forces on the cylinder. A detailed description of this approach is given by Rockwell *et al.* (1993). A continuous argon-ion laser, having a maximum power output of 25 W, passed through an optical train, then impinged upon a rotating, multi (48)-faceted polygon mirror. The effective scanning rate of the laser beam was either 150 cycles s^{-1} or 300 cycles s^{-1}, depending on the value of the free-stream velocity. Seeding was accomplished using 12 μm silver-coated particles. Multiply-exposed images of these particles were attained using a motor-driven 35 mm camera, which allowed acquisition at a rate of 5.6 frames per second, corresponding to 20 frames over the oscillation cycle. High resolution (300 lines)/mm film was used. In order to avoid the difficulties of directional ambiguity of the particle image pattern, a bias (rotating) mirror was located in front of the camera lens. The effective angle of rotation of the mirror was much smaller than 1°, thereby precluding systematic distortion errors. The 35 mm negatives were digitized at a resolution of 125 pixels mm^{-1}. The digitized pattern of particle images was then evaluated using a single-frame, cross-correlation technique with a window size of 90 pixels to yield the velocity field. The criterion of high-image-density was well exceeded by ensuring that a minimum of approximately 50 particle images was maintained within the interrogation window; this large number of images optimizes the sharpness of the correlation peaks. A 50% overlap was employed during the interrogation process. The magnification of the camera lens was $M = 1:6$, yielding an effective grid size on the 35 mm negative of 0.36 mm × 0.36 mm; in the plane of the laser sheet, the grid size was 2.1 mm × 2.1 mm. Post-processing of the velocity field yielded distributions of instantaneous vorticity. The uncertainty of the vorticity values depends on the spatial location, i.e. in regions of large mean vorticity uncertainty will be relatively high. The maximum value of uncertainty, accounting for bias and random errors, is estimated to be 4%.

3. Spectra of forces

Figure 1 exhibits spectra of the transverse force coefficient C_y as a function of the ratio of the cylinder oscillation frequency f_e to the Kármán shedding frequency f_0 from the corresponding stationary cylinder. The excerpts shown in figure 1 are from a larger number of spectra over the indicated range of f_e/f_0. The occurrence of locked-on states of asymmetrical vortex shedding in the near wake is suggested by spectra with large-amplitude sharply defined peaks. At $f_e/f_0 = 0.44$, three sharp spectral peaks are evident; the predominant peak is at a frequency corresponding to the third harmonic of the cylinder oscillation frequency, i.e. $f/f_e = 3.0$. Increases

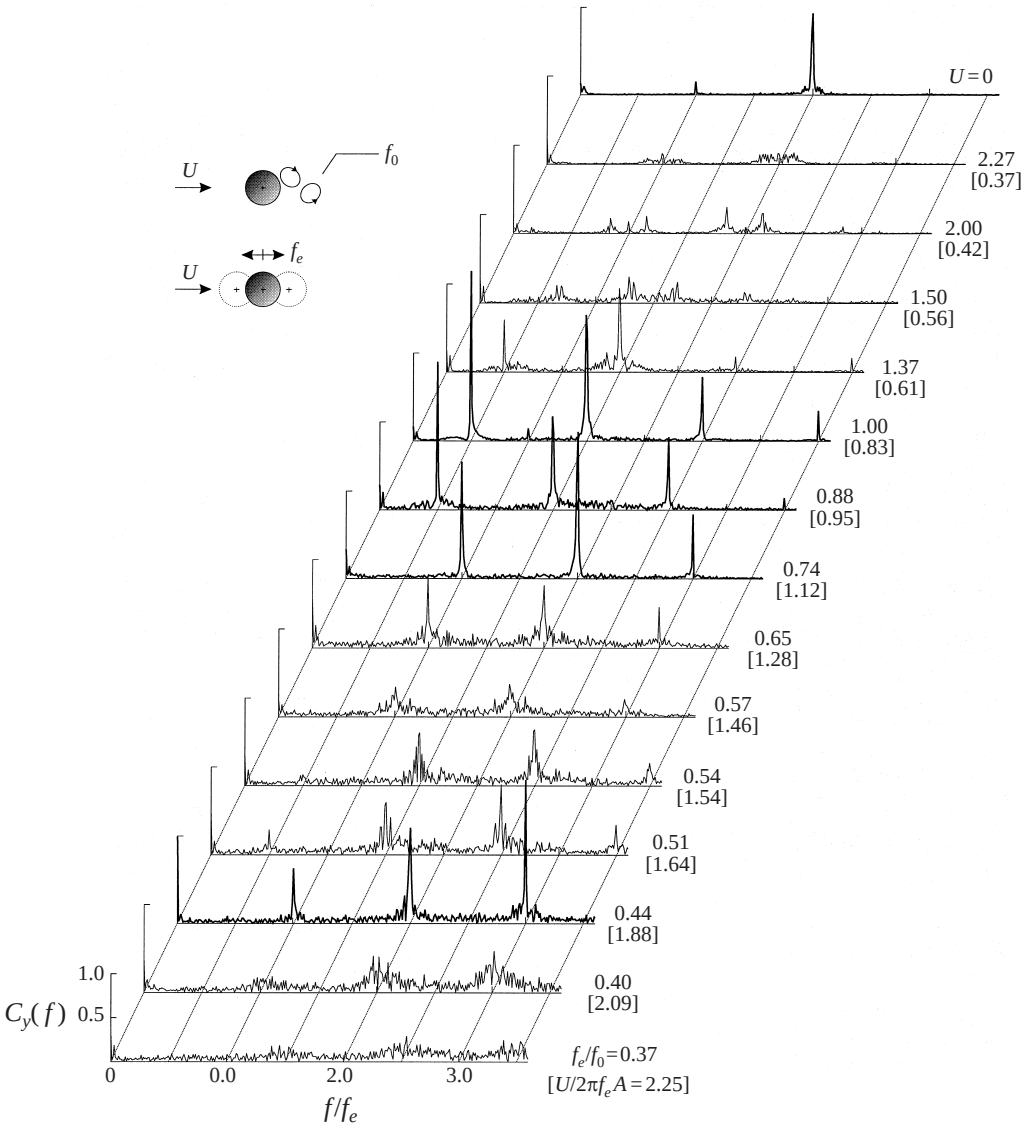

FIGURE 1. Spectra of transverse force coefficient over a range of excitation frequency f_e relative to the inherent frequency f_0 of Kármán vortex formation from the corresponding stationary cylinder.

in dimensionless excitation frequency f_e/f_0 produce lower-amplitude broader-band peaks for $f_e/f_0 = 0.51$ and 0.54; in fact, these broadband peaks are downshifted to values of $f/f_e = 1.5$ and 2.5. Further increases of the excitation frequency to $f_e/f_0 = 0.57$ and 0.65 produce a further downshift of the detectable peaks to $f/f_e = 1.0$ and 2.0 and, correspondingly, the tendency towards increasingly sharp spectral peaks, particularly evident at $f_e/f_0 = 0.65$. This process culminates at $f_e/f_0 = 0.74$, where well-defined large-amplitude spectral peaks occur, with the predominant one being at $f/f_e = 2.0$. A still further increase to $f_e/f_0 = 0.88$ yields continued downshifting of the predominant spectral peaks, with the predominant one now occurring at $f/f_e = 0.5$ for both $f_e/f_0 = 0.88$ and 1.0. Finally, over the remaining range of

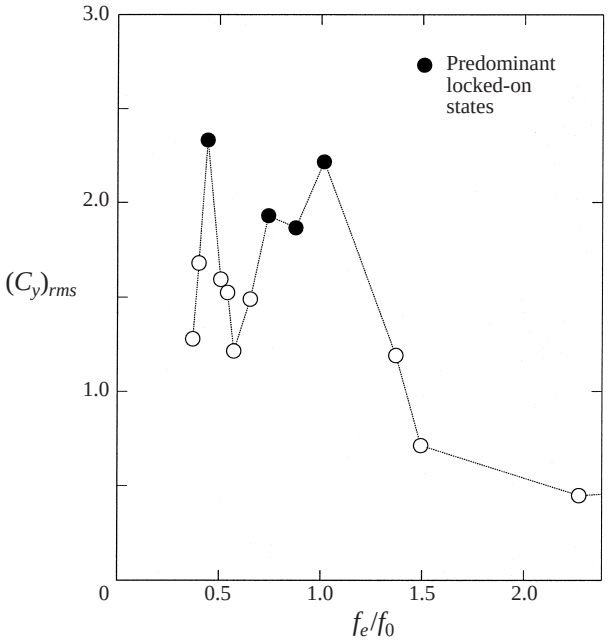

FIGURE 2. Variation of root-mean-square (r.m.s.) values of transverse force coefficient $(C_y)_{rms}$ over a range of dimensionless excitation frequency f_e/f_0, in which f_0 is the frequency of Kármán vortex formation from the corresponding stationary cylinder.

cylinder oscillation frequencies, there is actually an upshifting of the detectable, typically broadband, peaks to higher frequencies. As a reference, the spectrum for the limiting case of cylinder oscillation in quiescent fluid, i.e. $U = 0$, is illustrated; the predominant peak occurs at $f/f_e = 2.0$.

In summary, the foregoing observations of the spectra indicate a remarkable downward shift to lower frequencies of the predominant spectral peaks as the cylinder excitation frequency is increased to $f_e/f_0 = 1.0$. Over this range, the frequency of the predominant spectral peak decreases by a factor of 6, even though the dimensionless frequency of the cylinder oscillation f_e/f_0 increases by a factor of approximately 2. Moreover, these spectra suggest that locked-on states of the antisymmetrical mode of vortex formation occur at approximately the subharmonic $f_e/f_0 = 0.44$, near the fundamental, $f_e = 0.74$ and 0.88, and at the fundamental, $f_e/f_0 = 1.0$, of the Kármán shedding frequency from the corresponding stationary cylinder. In addition, in the limiting case of no current, the sharp spectral peak also indicates occurrence of persistent, locked-on vortex formation in the antisymmetrical mode. Despite the variations of velocity amplitude ratio $U/2\pi f_e A$ indicated in figure 1, the predominant parameter that determines the occurrence of lock-on is the frequency ratio f_e/f_0, i.e. it occurs at ratios corresponding to the subharmonic and fundamental of the Kármán frequency. Of course, this observation is limited to the ranges of parameters addressed herein.

The variation of the root-mean-square (r.m.s.) of the transverse force coefficient $(C_y)_{rms}$ is shown in figure 2. Peak values occur at $f_e/f_0 = 0.44$ and 1.0, henceforth referred to as approximately subharmonic and fundamental oscillations of the cylinder. These peaks correspond to locked-on states of the flow, designated by the filled circular symbols. Additional locked-on states occur as the limit $f_e/f_0 = 1.0$ is ap-

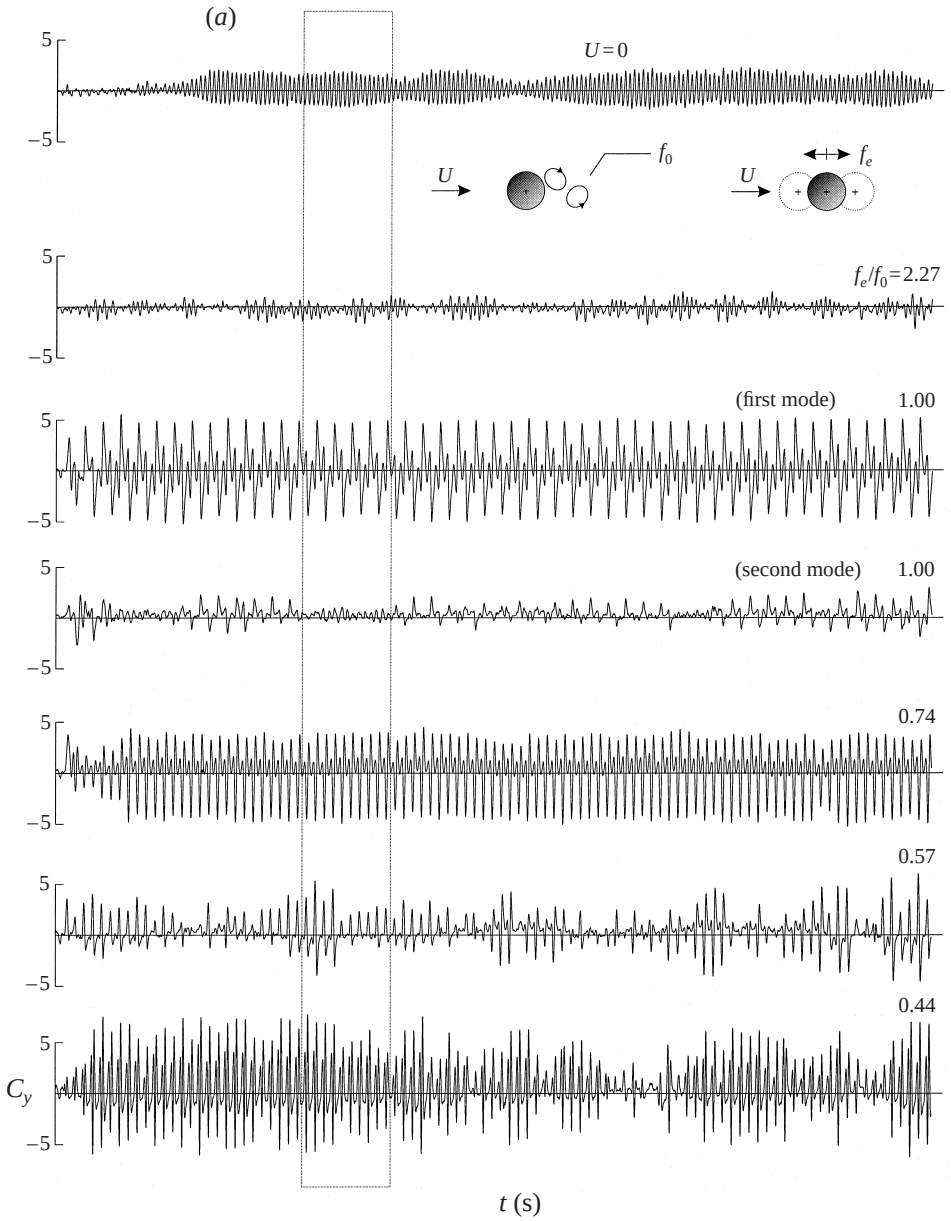

FIGURE 3(*a*). For caption see facing page.

proached, i.e. at $f_e/f_0 = 0.74$ and 0.88. All of these largest values of $(C_y)_{rms}$, which are hypothesized to represent locked-on states, correspond remarkably well to the bold spectra of figure 1, which exhibit sharply defined peaks.

A proper understanding of the origin of the foregoing spectra and r.m.s. values of the fluctuating transverse force coefficients requires consideration of the instantaneous force traces and the corresponding flow structure in the near wake of the cylinder. In the following, these features are addressed.

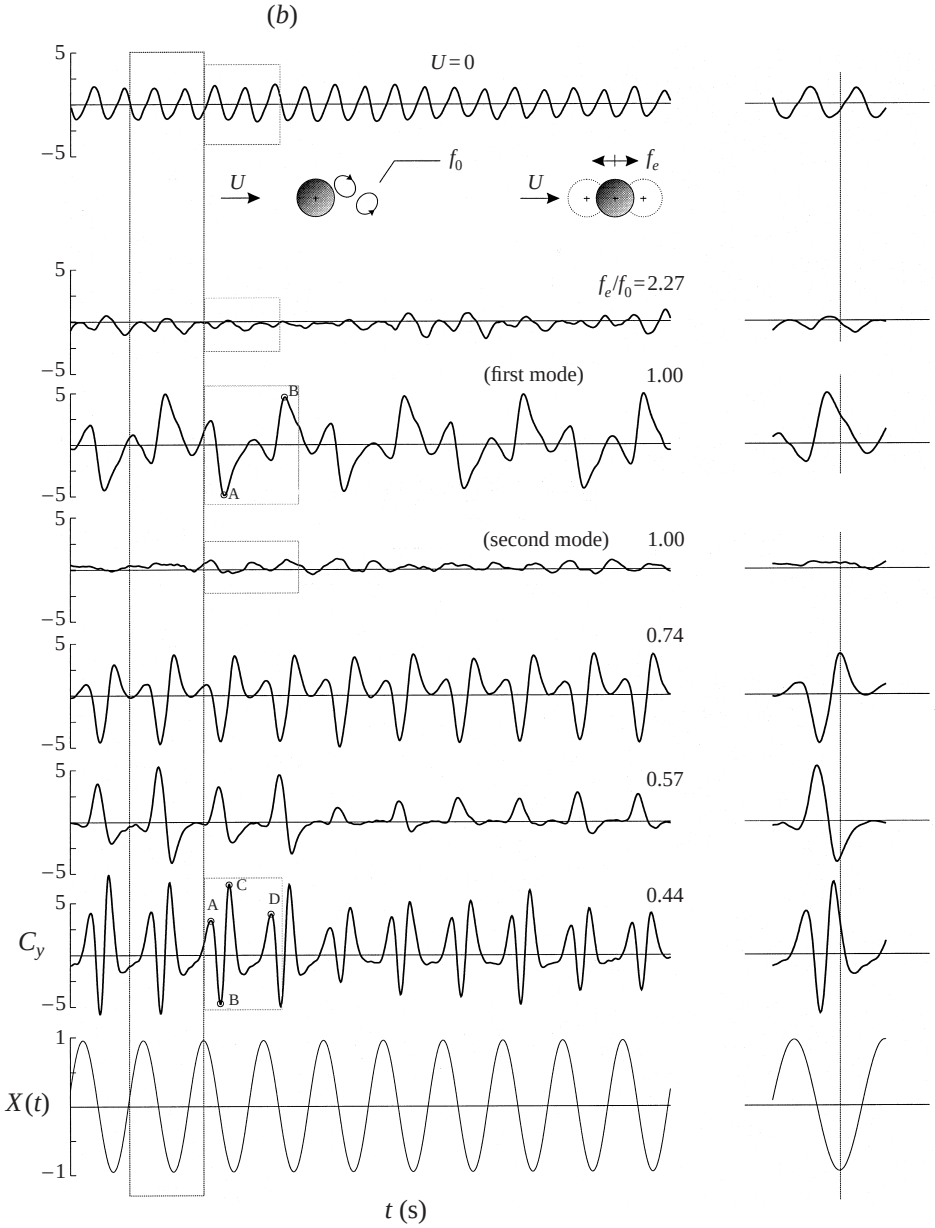

FIGURE 3. (*a*) Time traces of transverse force coefficient $C_y(t)$ corresponding to spectra of figure 1. (*b*) Expanded representations of portions of traces of (*a*). Excerpts in right column indicate phases of $C_y(t)$ relative to $X(t)$.

4. Instantaneous force traces

The time history of the fluctuating lift coefficient over 102 cycles of the cylinder oscillation is shown in figure 3(*a*) for selected values of cylinder excitation frequency f_e/f_0. Taking an overview of the traces of figure 3(*a*), it is clear that cylinder excitation at the near fundamental, $f_e/f_0 = 0.74$, and the fundamental, $f_e/f_0 = 1.0$ (first mode), of the inherent Kármán frequency produce the repetitive signatures of $C_y(t)$ of longest duration. It is, however, possible to identify extended regions of persistent patterns in

the lift traces at $f_e/f_0 = 0.44$. On the other hand, at values of $f_e/f_0 = 0.57$ and 2.27, corresponding to the minima in the plot of figure 1, generally intermittent fluctuations of $C_y(t)$ occur, with segments of repetitive lift fluctuations. It should be noted that it was possible to generate one of two modes at $f_e/f_0 = 1.0$, designated as first and second modes in figure 3(*a*); the first mode, giving rise to highly repetitive fluctuations of $C_y(t)$, was by far the predominant one. The existence of two admissible modes may be related to a process of nonlinear bifurcation that yields two branches of solution; this aspect deserves further consideration from a theoretical standpoint.

In order to obtain a more detailed view of the patterns of these instantaneous traces of $C_y(t)$, excerpts corresponding to the region defined by the rectangular box in figure 3(*a*) are exhibited in expanded form in figure 3(*b*). Therein, the trace of the cylinder displacement $x_c(t)$ is also shown for purposes of establishing a phase reference. In the right-hand column of figure 3(*b*), a further expanded segment of each trace of $C_y(t)$ is shown; a vertical reference line passes through the minimum of the $x_c(t)$ trace. It is evident that as the form of the trace of $C_y(t)$ changes with f_e/f_0, the location of instantaneous peaks and valleys is altered relative to the maximum negative value of $x_c(t)$.

Time histories of the instantaneous in-line force coefficient $C_x(t)$ over long records, analogous to those shown in figure 3(*a*), show generally repetitive, i.e. locked-on, characteristics and only mild amplitude modulations are discernible. In addition, the corresponding spectra for all traces have a predominant frequency corresponding to the oscillation frequency f_e of the cylinder. As a consequence, they are not shown here.

Instantaneous, expanded traces of $C_x(t)$ are shown in figure 4. At $f_e/f_0 = 0.44$, the mean value of the in-line force coefficient $\bar{C}_x$ is relatively high; it has a value $\bar{C}_x = 5.77$. As the cylinder oscillation frequency f_e/f_0 is increased, both the amplitude of $C_x(t)$ and the averaged coefficient $\bar{C}_x$ tend to decrease, attaining their asymptotic value at $f_e/f_0 = 2.27$. In the right-hand column of figure 4, the vertical line passing through excerpts of the $C_x(t)$ traces provides an indication of the instantaneous phase of $C_x(t)$ with respect to the instantaneous cylinder displacement $x_c(t)$.

Further insight into the time history of the unsteady loading, relative to the motion of the cylinder, is given in the Lissajous patterns of figure 5. These patterns were constructed from 12.5 cycles of the cylinder oscillation., i.e. only for a short segment of the entire $C_y(t)$ trace of figure 3(*a*). At a given value of dimensionless oscillation frequency f_e/f_0 of the cylinder, plots of $C_y(t)$ versus $x_c(t)$, $C_x(t)$ versus $x_c(t)$, and $C_y(t)$ versus $C_x(t)$ are illustrated for a total of 12.5 oscillation cycles of the cylinder. At the lowest frequency ratio, $f_e/f_0 = 0.44$, it is evident from inspection of the plot of $C_y(t)$ versus $x_c(t)$ that truly locked-on, i.e. phase-locked, behaviour of the cylinder loading, and implicitly the near-wake structure, are not achieved. Indeed, this plot shows substantial variations over a large number of cycles. The shaded region corresponds to clockwise portions of the trajectory, i.e. positive hysteresis loops. It is evident that over selected cycles of the cylinder oscillation, relatively large positive hysteresis occurs. Similarly, negative hysteresis corresponds to the counterclockwise portion of the C_y versus $x_c(t)$ loop. At a higher frequency ratio, $f_e/f_0 = 0.57$, the overall plot $C_y(t)$ versus $x_c(t)$ suggests a non-phase-locked state. It should be noted that, at $f_e/f_0 = 0.57$, different forms of Lissajous patterns were obtained for different segments of the longer time trace of $C_y(t)$ in contrast to the case of $f_e/f_0 = 0.44$. As a result, the degree of phase-locking at $f_e/f_0 = 0.57$ is substantially less than that conveyed by the pattern of figure 5(*a*). Attainment of highly repetitive phase-locked states is evident at the higher values of frequency ratio $f_e/f_0 = 0.74$ and 1.0. At $f_e/f_0 = 0.74$, the magnitude of positive hysteresis is very large, whereas at

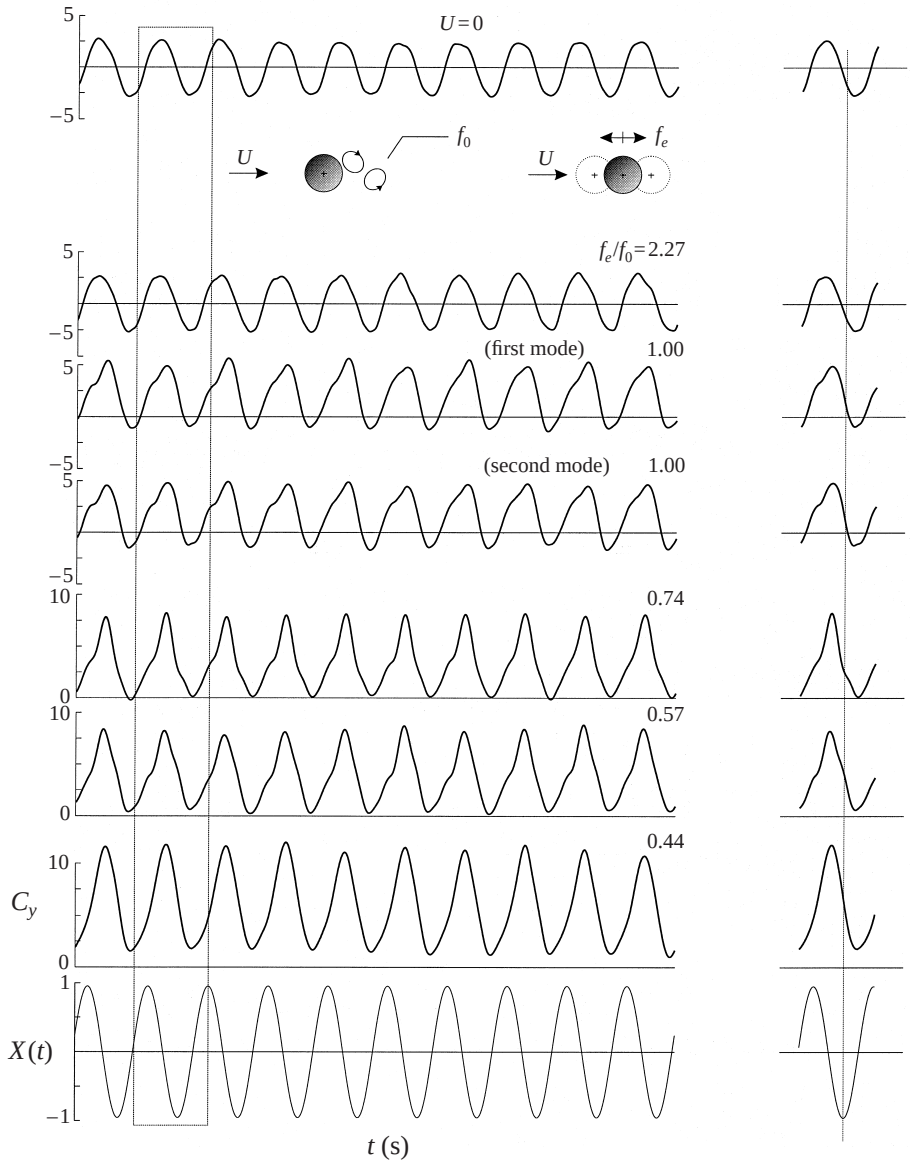

FIGURE 4. Expanded representations of traces of in-line force coefficients for selected values of excitation frequency f_e normalized by frequency f_0 of inherent Kármán vortex formation.

$f_e/f_0 = 1.0$, it is substantial but, due to the symmetry and high degree of repeatability of the $C_y(t)$ versus $x_c(t)$ trajectory, it has a form that is essentially a mirror image of the corresponding negative loop. For the alternate, second mode at $f_e/f_0 = 1.0$, represented by the bottom plots of figure 5(*b*), non-phase-locked behaviour is evident, again corresponding to the non-repeating nature of the C_y versus $x_c(t)$ trace. A similar conclusion holds for the frequency ratio $f_e/f_0 = 2.27$. For the limiting case of no mean flow, however, shown in the top row of figure 5(*b*), phase-locked behaviour is clearly evident in the C_y versus $x_c(t)$ plot. Again, the positive hysteresis loop is nearly the mirror image of the corresponding negative loop.

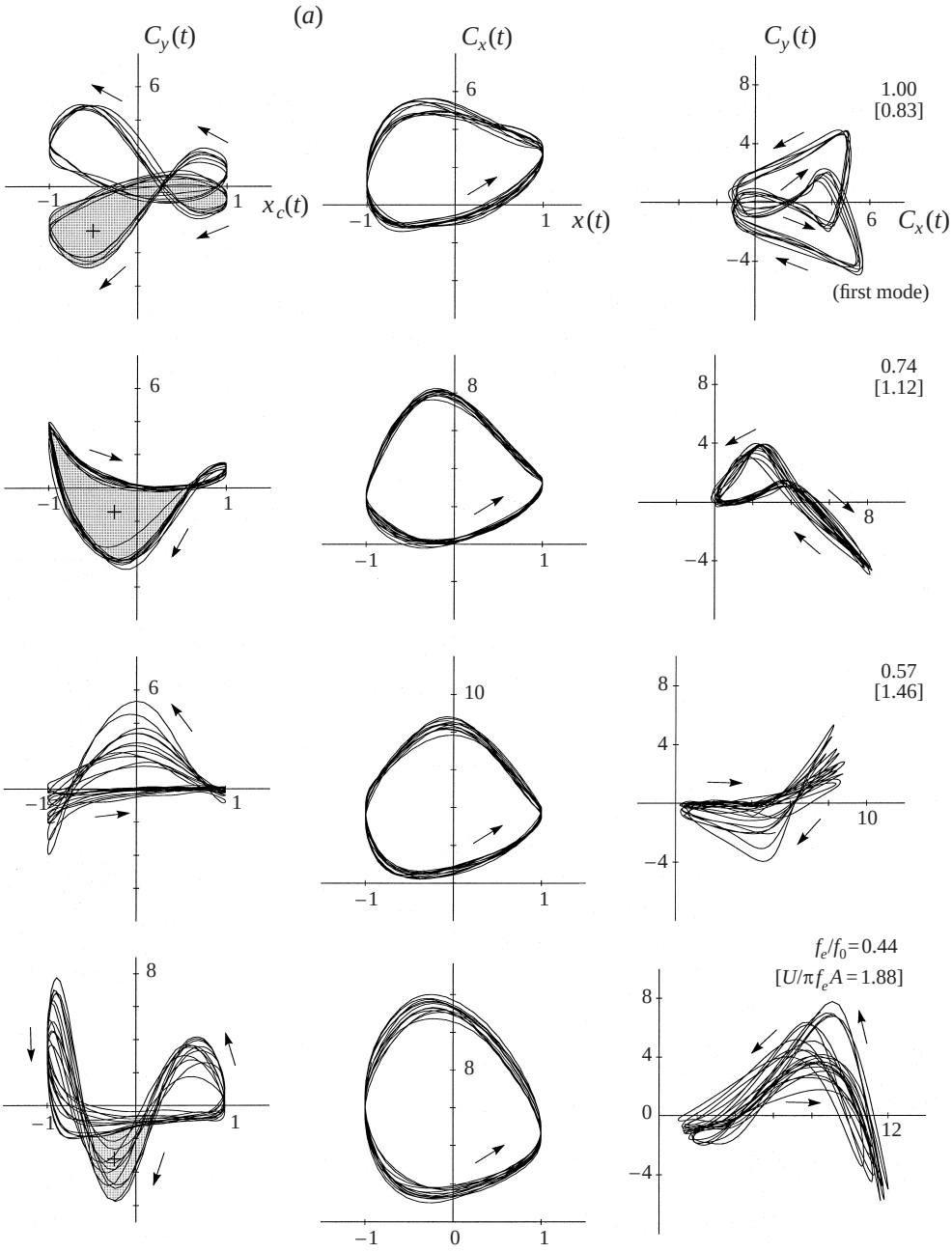

FIGURE 5(*a*). For caption see facing page.

Viewing together all of the plots of figures 5(*a*) and 5(*b*), it is evident that all trajectories $C_x(t)$ versus $x_c(t)$ exhibited in the middle column are highly repetitive and essentially congruent. For the traces of $C_y(t)$ versus $C_x(t)$ in the right-hand column, the degree of phase-locking, or, in other words, the magnitude of the cycle-to-cycle

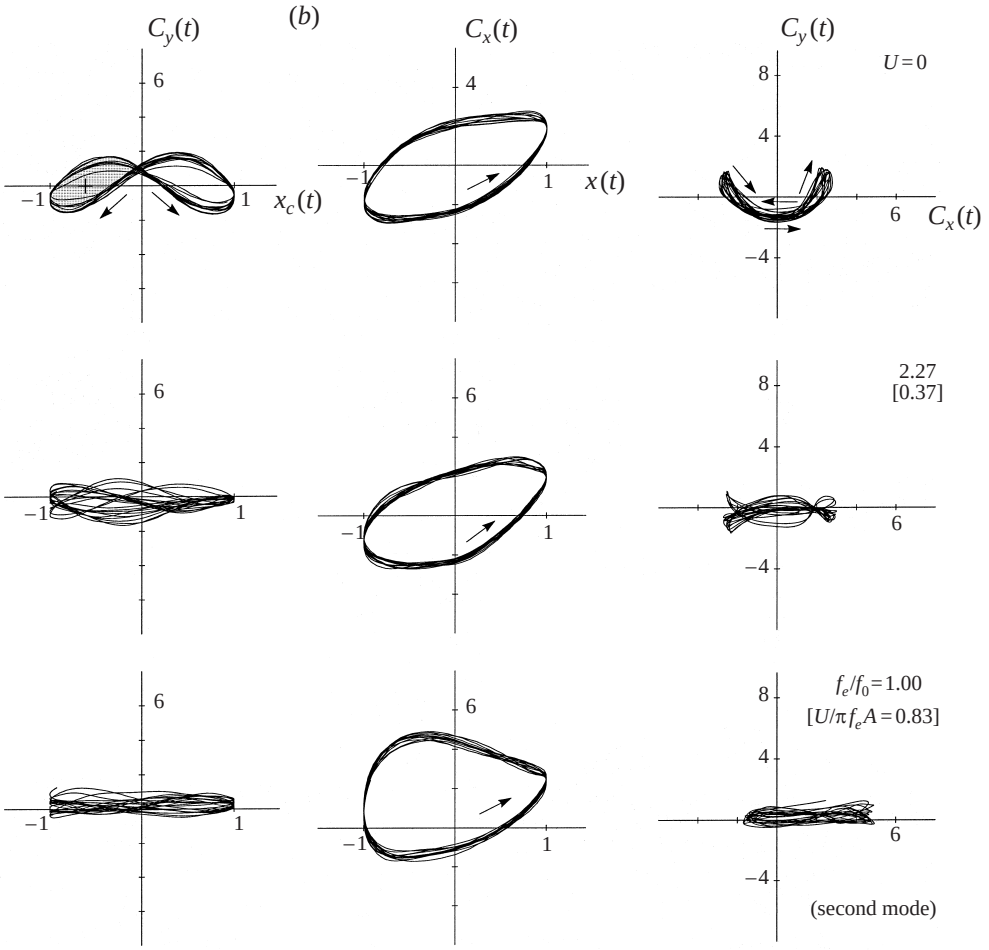

FIGURE 5. Representations of transverse and in-line force coefficients $C_y(t)$ and $C_x(t)$ at selected values of excitation frequency f_e normalized by inherent vortex formation frequency f_0 from the corresponding stationary cylinder.

phase deviation is therefore attributable to that of the corresponding $C_y(t)$ versus $x_c(t)$ traces shown in the left-hand column.

Concerning the effect of variation of KC on the appearance of the Lissajous patterns, some preliminary data, not included herein, can provide further insight. At a frequency ratio $f_e/f_0 = 0.44$, the most organized and persistent patterns of Lissajous trajectories were obtained at $KC = 6$, and those at $KC = 4$, 8 and 10 were generally less organized, suggesting a tendency towards a lower degree of lock-on. On the other hand, at a frequency ratio $f_e/f_0 = 1.0$, the Lissajous trajectories were highly ordered at all values of $KC = 4$, 6, 8 and 10, with the largest deviations occurring at $KC = 10$. Although the detailed form of these trajectories varied somewhat, it appears that locked-on patterns are generally attainable over a range of KC. It should be noted that the degree of organization of these Lissajous patterns are reflected in the corresponding spectra at these values of KC, which will be addressed in conjunction with figure 12.

5. Basic modes of vortex patterns in the near wake

The remarkable features of the time traces, spectra and Lissajous patterns of the instantaneous transverse $C_y(t)$ and in-line $C_x(t)$ coefficients addressed in the foregoing have their genesis in the vorticity field of the cylinder wake. The basic modes of the near-wake vorticity patterns, with emphasis on locked-on states, are described in the following. Excerpts from cine sequences are correlated directly with the instantaneous transverse force coefficient $C_y(t)$, the cylinder displacement $x_c(t)$, and the instantaneous relative velocity $U - U_c(t)$.

5.1. *Mode due to subharmonic oscillation*

Figure 6 shows the case of the subharmonic oscillation, approximated as the frequency ratio $f_e/f_0 = 0.44$, which gives maximum spectral peaks and value of r.m.s. amplitude in the immediate vicinity of $f_e/f_0 = 0.5$ (see figures 1 and 2). The inset of figure 6 shows slightly more than one complete cycle of the repetitive $C_y(t)$ trace; this trace corresponds to the portion of the trace of figure 3(*b*) with peaks designated A, B, C, D. Corresponding variations of the cylinder displacement $x_c(t)$ and relative velocity $U - U_c(t)$ are indicated. Frames extracted from the cine sequence are designated as $N = 3, 4, 5$ and so on. The corresponding instantaneous values of $U - U_c(t)$ and $x_c(t)$ are indicated by the hollow symbols. Instantaneous patterns of negative (thin line) and positive (thick line) vorticity in the sequence of images show the relationship between the evolution of the near-wake structure and the instantaneous value of $C_y(t)$. Images $N = 3, 4$, and 5 show patterns near maximum negative C_y, which occurs approximately at $N = 4$. In this series, the upper, fully formed negative vortex moves up and away from the surface of the cylinder, while the positive lower vortex continues to develop near the base region. On the other hand, images $N = 6, 7$, and 8 show an approximate inversion of this process; that is, the fully formed positive vortex from the lower surface of the cylinder moves away from it, while the upper negative vortex continues to form near the base. These basic features of the near wake and the occurrence of negative and positive peaks in the C_y trace are in accord with the reasoning of Maull & Milliner (1978), based on simplified point-vortex simulation and qualitative visualization; for example, movement of the negative, fully formed vortex away from the upper surface of the cylinder contributes to a negative peak of C_y and conversely for the fully formed vortex from the lower surface of the cylinder.

Taken together, the images $N = 4$–8 of figure 6 represent approximately one half-cycle of Kármán-like shedding. As seen from the plot of $U - U_c$ in the inset, this type of shedding occurs at relatively high values of relative velocity $U - U_c(t)$, which correspond to zero or negative values of cylinder displacement $x_c(t)$.

On the other hand, images $N = 13$, 15, and 18 illustrated in the right-hand column depict a fundamentally different scenario. Comparing images $N = 13$ and 15, it is clear that the approximate position and form of the positive vorticity concentration formed from the lower surface of the cylinder, as well as the negative vorticity layer and concentration from the upper surface of the cylinder, undergo very little change in form and position. Moreover, the larger-scale positive concentration of vorticity evident in the lower right-hand corner of these images shows little change of position relative to the cylinder. In an approximate sense, one may therefore view the near-wake pattern as effectively 'frozen'. Referring to the inset of figure 6, this so-called frozen structure of the near wake occurs for minimum values of relative velocity $U - U_c$. In contrast, rapid changes of the near-wake vorticity patterns occur over the same time interval for images $N = 3$ to 5. If the near-wake pattern of vorticity is strictly 'frozen', then the patterns of vorticity do not change with time. In this

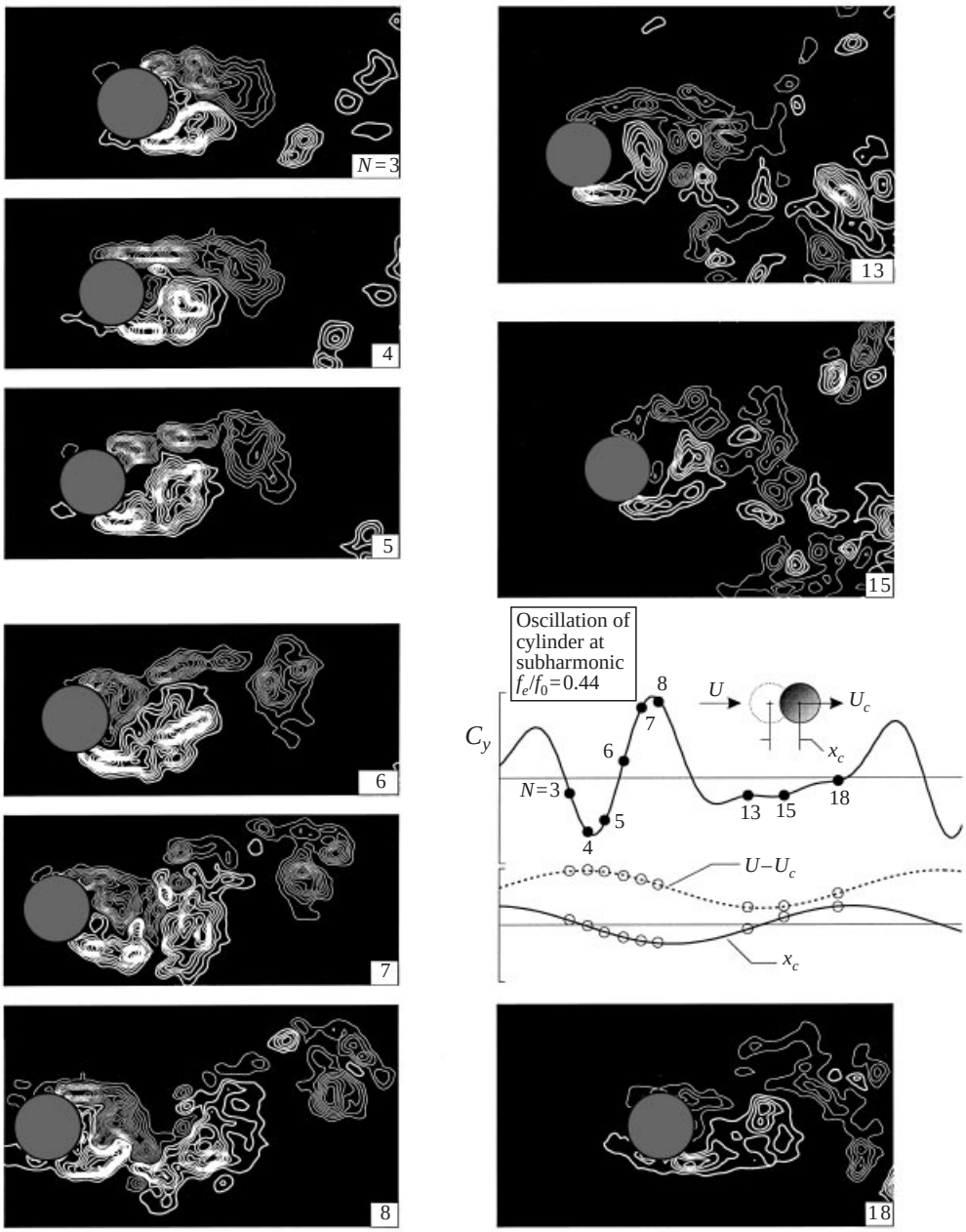

FIGURE 6. Instantaneous patterns of vorticity over a cycle of oscillation of the cylinder at approximately the subharmonic of the Kármán shedding frequency, i.e. $f_e/f_0 = 0.44$. Patterns of vorticity are correlated with the time variation of the transverse force coefficient $C_y(t)$, the cylinder displacement $x_c(t)$, and the difference between the free-stream velocity U and the cylinder velocity $U_c(t)$, i.e. $U - U_c(t)$.

limiting case, the concept of Lighthill (1986), which relates the induced force to the time rate change of moments of vorticity, indicates that the induced lift will be zero. As indicated on the trace of C_y, at $N = 13$ and 15, the lift is small, but not zero, meaning, of course, that the entire wake structure, including that downstream of the

field of view, varies somewhat. Moreover, to illustrate further the very slow changes in the near-wake vorticity field, an image corresponding to $N = 18$ is also shown. Significant, but still relatively small, changes in the location and form of the positive and negative regions of vorticity are evident, relative to those at $N = 13$ and 15. In summary, the time interval of five frames extending from $N = 13$ to 18 is the same time interval as for images $N = 3$ to 8. Yet, the rate of change of both the vorticity patterns and the C_y trace is dramatically different for these two intervals.

Viewing figure 6 as a whole, it is evident that the occurrence of Kármán vortex formation over a fraction of the oscillation cycle of the cylinder, and a nearly frozen pattern of near-wake vortices over the remaining portion of the cycle, dictate the detailed form of the time trace of C_y. In fact, the time lapse between the occurrence of the first two positive peaks of C_y in the inset of figure 6 is 0.32 $T_e = 0.32/f_e$, where T_e is the period of the cylinder oscillation. In other words, the Kármán process of shedding, which produces the major positive and negative peaks of C_y, occurs over approximately one-third of the total period T_e. Referring to the spectra of figure 1, the predominant spectral peak occurs at $f_e/f_0 = 3.0$. This peak is therefore due to the occurrence of Kármán-like shedding only over one-third of the total oscillation cycle.

5.2. *Mode due to fundamental oscillation*

The case of cylinder oscillation at the fundamental of the Kármán frequency, i.e. $f_e/f_0 = 1.0$, is shown in figure 7. Images $N = 8$ to 12 show movement of both the negative, large-scale concentration of vorticity and the negative distributed-layer vorticity away from the cylinder; simultaneously, development of the positive vorticity concentration from the lower surface of the cylinder continues. In images $N = 28$, 30 and 32, the converse scenario occurs. In accord with the reasoning of Maull & Milliner (1978), these near-wake changes in patterns of vortex patterns should, for $N = 8$ to 12, contribute to a negative peak of C_y and for $N = 28$ to 32, to a positive peak of C_y. The trace of C_y shown in the inset of figure 7 shows that this is indeed the case. This trace represents an excerpt from the extended signature of figure 3(*b*), with peaks designated A and B. In contrast to the case illustrated in figure 6, the two stages of the Kármán-like vortex shedding do not occur consecutively. Rather, they are interrupted by the nearly frozen wake structure shown in images $N = 18$, 20 and 22 in the right-hand column. Discernible, nevertheless small, changes in the form and location of positive and negative concentrations of vorticity occur over this time span, thereby producing the very small values of C_y indicated in the inset. Furthermore, it should be noted that the occurrence of the negative peak of C_y at $N = 10$ and the positive peak at $N = 30$ corresponds to an instantaneous value of relative velocity $U - U_c$ close to the maximum.

On the other hand, the essentially frozen wake structure in images $N = 18$ to 22 corresponds approximately to the minimum values of $U - U_c$. The fact that the two sequential stages of Kármán-like shedding are interrupted by the occurrence of frozen wake structure produces, in effect, an artificially long period of vortex formation in the near wake. The elapsed time between frames $N = 10$ and 30 in the insert represents approximately one-half period of the large-scale vortex formation in the near wake. This time increment also corresponds to the period $T_e = 1/f_e$ of the oscillation cycle of the cylinder. On the basis of these observations, one expects the predominant spectral peak of C_y to be at the subharmonic of the excitation frequency f_e. Indeed, as shown in the spectrum at $f_e/f_0 = 1.0$ in figure 1, the major peak is at $f/f_e = 0.5$.

A direct comparison of key features of the wake structure, along with traces and spectra of C_y, is given in figure 8 for the cases of subharmonic and fundamental

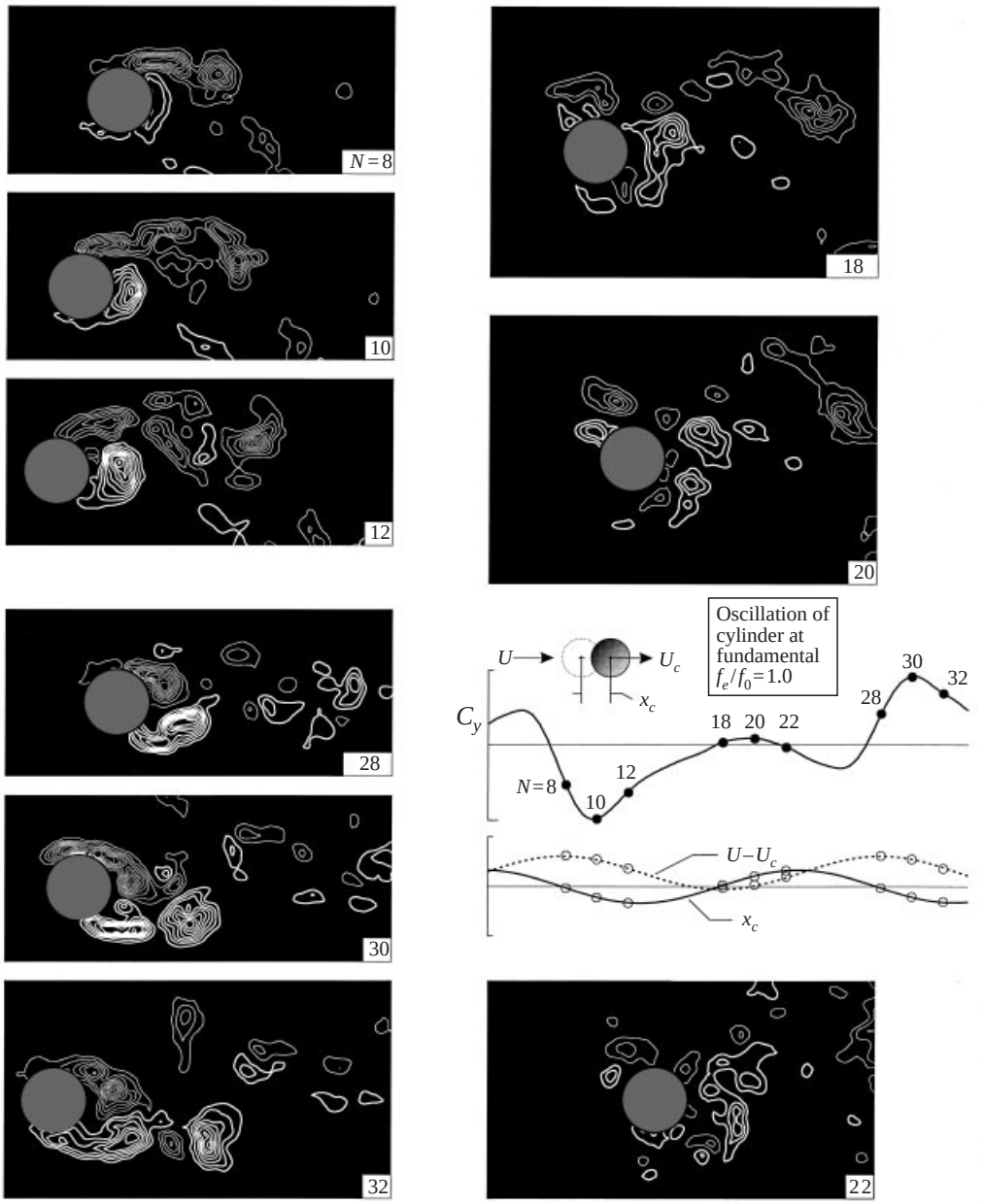

FIGURE 7. Instantaneous patterns of vorticity over a cycle of oscillation of the cylinder at the fundamental of the Kármán shedding frequency, i.e. $f_e/f_0 = 1.0$. Patterns of vorticity are correlated with $C_y(t)$, $x_c(t)$, and $U - U_c(t)$.

excitation. This comparison underscores the radical alterations of the spectral content of the loading that can be induced by variations in timing of Kármán-like vortex formation.

During the course of the experiments, the predominant mode of vortex formation due to fundamental excitation was as indicated in figure 7. As noted previously, this predominant mode is designated as the first mode. During certain start-ups of the

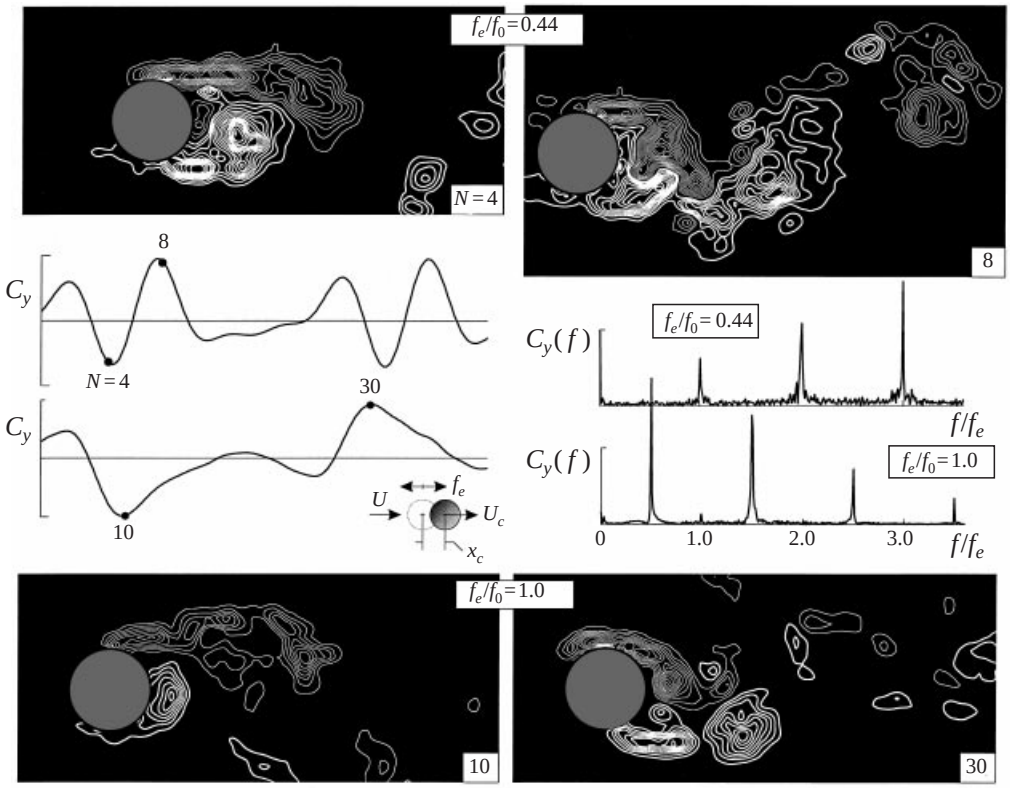

FIGURE 8. Direct comparison of patterns of vorticity with temporal variations and spectra of the transverse force coefficient C_y for oscillation of the cylinder at the approximate subharmonic and fundamental frequencies, $f_e/f_0 = 0.44$ and 1.0.

experiment, apparently for slightly different initial conditions, a second mode was also observed, albeit much less frequently. It is shown in comparison with the first mode in figure 9. The prevalent feature of this second mode, represented by the images in the second column, is a tendency to form a symmetrical pattern of vortices during those stages of the cylinder oscillation that normally give rise to Kármán-like shedding for the first mode, represented in the first column. This tendency towards symmetry, at least for the patterns of vorticity immediately surrounding the cylinder, is maintained during the portion of the cycle for which the wake tends to remain effectively frozen, indicated by image $N = 20$ in the second column of figure 9.

The occasional onset of the symmetrical mode is replaced by a persistent version of this mode when the cylinder oscillates at the first harmonic of the Kármán frequency, $f_e/f_0 = 2$, represented by the images and traces of C_x and C_y shown in figure 10(*a*). Symmetry of the patterns of positive and negative vorticity is maintained at the maximum and minimum values of reduced velocity $U - U_c$. Due to this symmetry, the magnitude of the trace C_y remains very small, whereas that of C_x exhibits relatively large positive and negative values at the maximum and minimum values of $U - U_c$.

Finally, the limiting case of oscillation in the absence of mean flow, corresponding to the case of $U = 0$, produces asymmetrical patterns of vorticity, yielding a repetitive signature of $C_y(t)$, shown in the inset of figure 10(*b*), which represents an excerpt from the trace of figure 3(*b*). This pattern of vortex formation was originally suggested

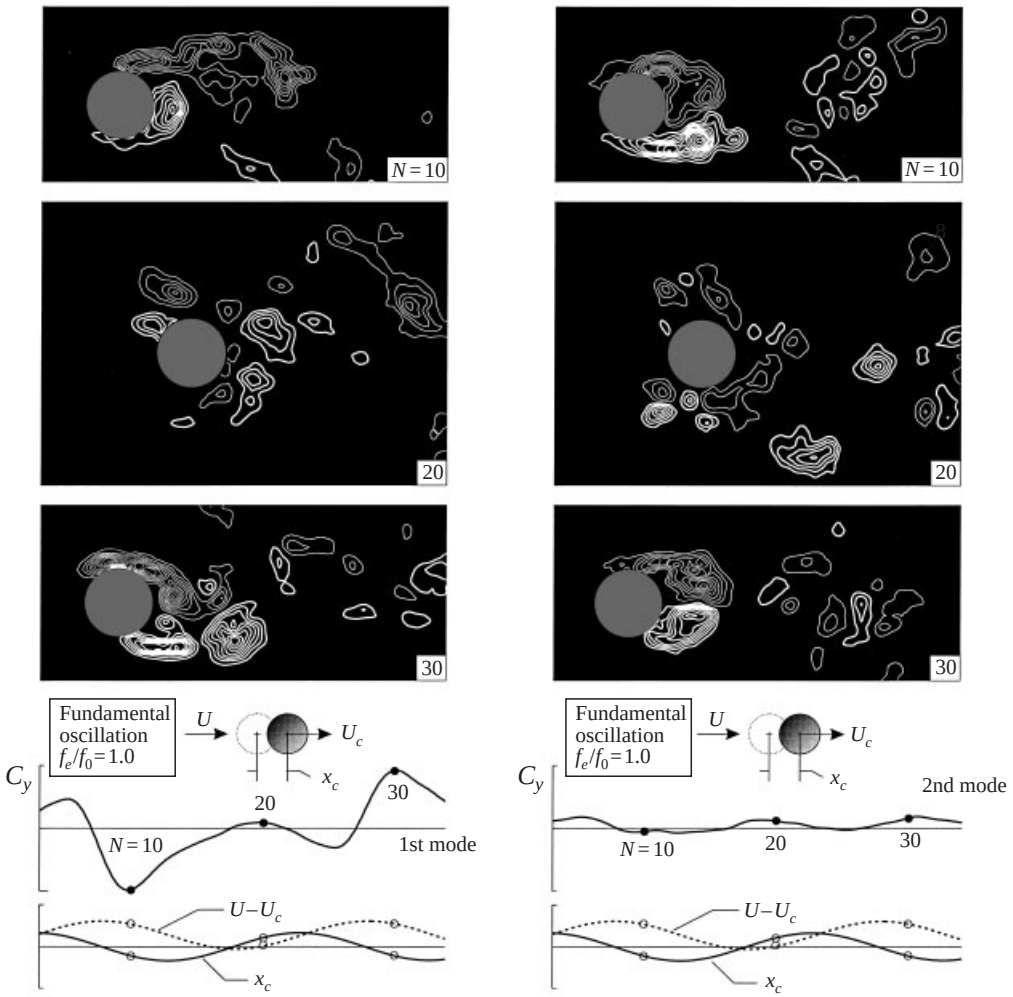

FIGURE 9. Illustration of two possible modes of locked-on vortex formation arising from oscillation of the cylinder at the inherent Kármán frequency, $f_e/f_0 = 1.0$. Patterns of instantaneous vorticity are correlated with $C_y(t)$, $x_c(t)$, and $U - U_c(t)$.

in the qualitative flow visualization of Obasaju *et al.* (1988); the magnitude and frequency of C_x and C_y are very close to their values.

6. Overview of force signatures and spectra

6.1. *Signatures of transverse force*

Figure 11 provides an overview of time traces of the transverse force coefficient C_y as a function of Keulegan–Carpenter number KC at three different values of frequency ratio f_e/f_0 and, in addition, for the limiting case of zero current $U = 0$. These traces were extracted from a much longer, continuous record of C_y. For certain cases, the longer trace exhibited intermittency between the organized traces shown in figure 11 and relatively disorganized oscillations; this issue will be addressed subsequently. First, consider the limiting case of cylinder oscillations in the absence of current, $U = 0$, shown in figure 11(*b*). It is evident that detectable fluctuations of C_y occur

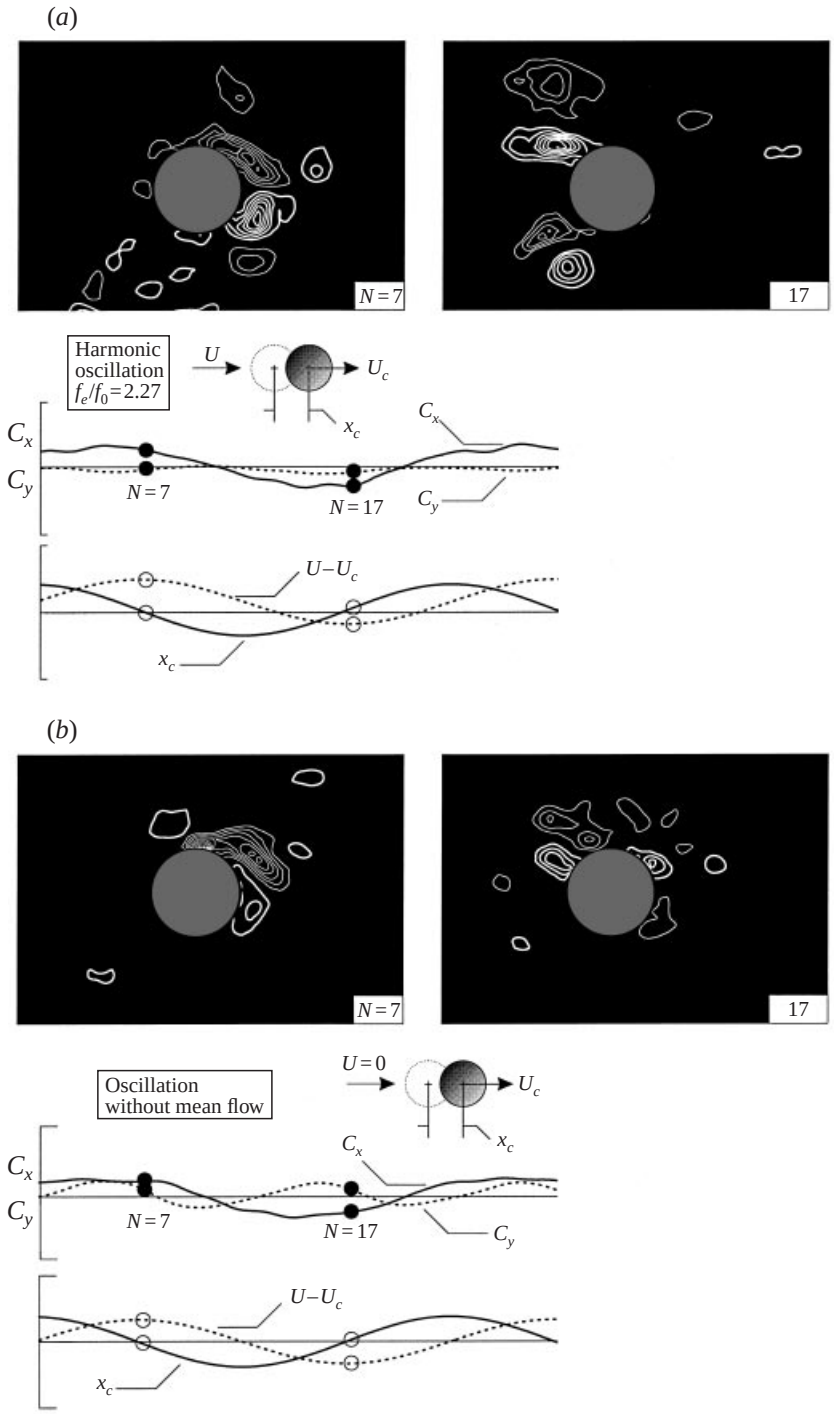

FIGURE 10. (*a*) Patterns of instantaneous vorticity corresponding to approximately harmonic oscillation of the cylinder at excitation frequency f_e normalized by inherent Kármán vortex formation frequency f_0, i.e. $f_e/f_0 = 2.27$. (*b*) Representative images for the case of oscillation without mean flow. In both cases, the in-line and transverse force coefficients $C_x(t)$ and $C_y(t)$ are shown as a function of time and correlated with $x_c(t)$ and $U - U_c$.

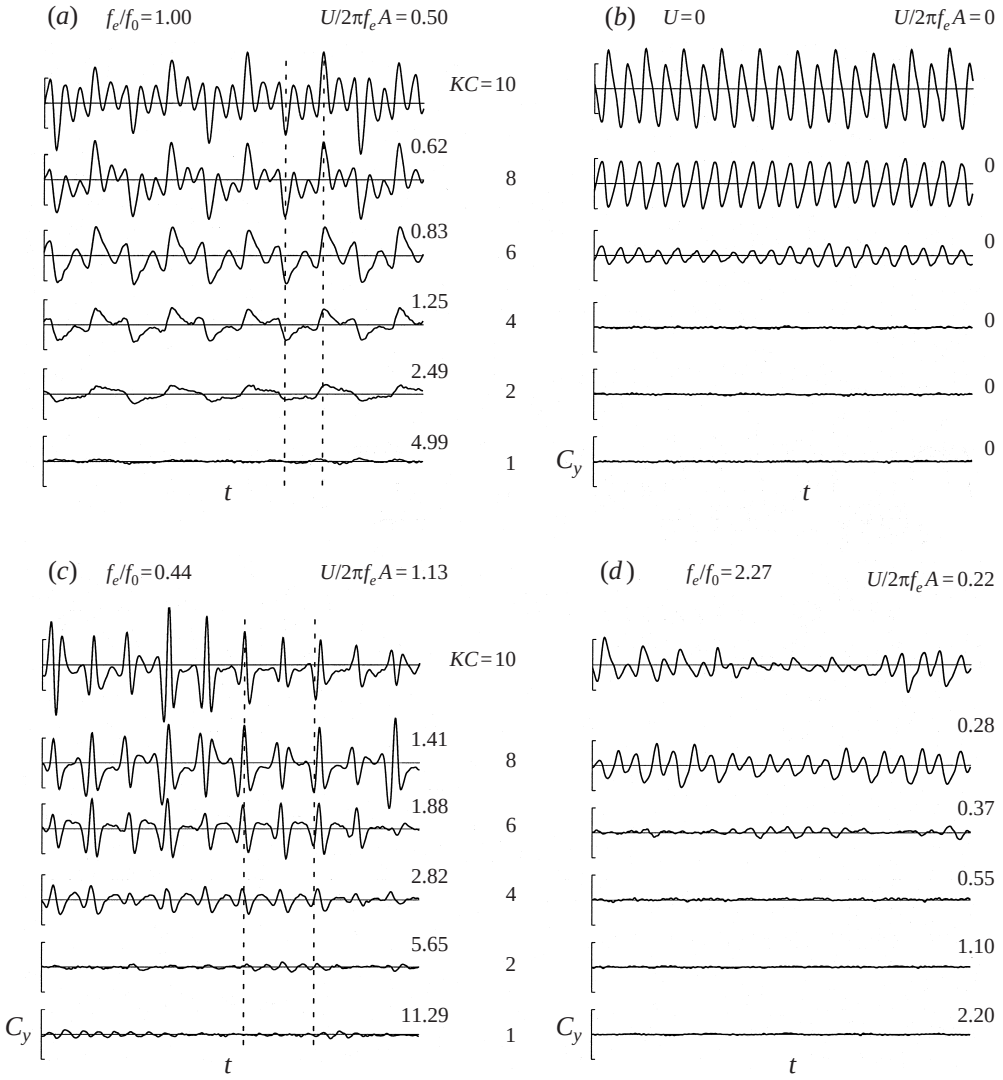

FIGURE 11. Overview of time traces of transverse force coefficient C_y at various values of frequency ratio f_e/f_0 and Keulegan–Carpenter number KC. These traces extend over ten cycles of the cylinder oscillation.

at $KC = 6$, and increase in magnitude for higher values of $KC = 8$ and 10. The predominant fluctuation component remains at the same frequency for all values of KC; it corresponds to a frequency of twice the oscillation frequency of the cylinder. The general form of the traces at $KC = 6$ and 10, as well as their magnitudes, are remarkably similar to those observed in the experiments of Obasaju *et al.* (1988) for oscillating flow past a stationary cylinder and at $KC = 10$ by Lin & Rockwell (1999) for an oscillating cylinder in quiescent fluid. Except for significant amplitude modulation at $KC = 10$, all traces for these cases $U = 0$ are approximately sinusoidal, in sharp contrast to cases with finite current $U \neq 0$, addressed in the following.

For the case $f_e/f_0 = 1.0$, represented by the traces exhibited in figure 11(*a*), pronounced modulations occur for all values of KC and, in fact, these traces show

a broadly similar form for $KC = 4$ to 10. At sufficiently high $KC = 8$ and 10, additional, higher frequency fluctuations become evident. Nevertheless, the occurrence of the predominant positive and negative spike, and the spacing between them, is persistent over the range $KC = 4$ to 10, corresponding to $2.82 \geqslant U/2\pi f_e A \geqslant 1.13$. This observation suggests that the vorticity patterns depicted in figure 7 will generally be present over this range, save for additional modulations to account for the higher frequency components at higher values of KC.

In a similar spirit, the traces at $f_e/f_0 = 0.44$, exhibited in figure 11(*c*), have a modulated form, which is, in several respects, persistent over the range $KC = 4$ to 10. Again, the major features of the vorticity patterns shown in figure 6 are anticipated to be present over this range of KC.

At $f_e/f_0 = 2.27$, shown in figure 11(*d*), consistent fluctuations of C_y set in only at a sufficiently high value of $KC = 8$. Detectable patterns of modulation are evident at $KC = 8$ and 10, but the amplitude and degree of consistency is not as evident as that for the aforementioned cases.

6.2. *Spectra of transverse force*

Spectra corresponding to the long time records, from which the traces of figure 11 were extracted, are shown in figure 12. These time records involved 102 cycles of the cylinder oscillation. For some cases they include highly coherent oscillations, such as those corresponding to the excerpts shown in figure 11, as well as relatively irregular fluctuations (not shown). The consequence of the irregularity will be to produce substantially broader-band peaks in the spectra.

Considering, first of all, the case of approximately subharmonic oscillation at $f_e/f_0 = 0.44$ in figure 12, it is evident that the same spectral peaks are detectable at $KC = 2$, 4, and 6. They correspond to $f/f_e = 1$, 2 and 3. At $KC = 8$, they occur at $f/f_e = 0.5$, 1.5, 2.5 and 3.5. The most sharply defined peaks occur at $KC = 6$ and 8. A further increase to $KC = 10$ produces substantial broadening of the spectrum. A small increase of the dimensionless excitation frequency to $f_e/f_0 = 0.5$ generates spectra at $KC = 8$ and 10 that are very similar to those at $f_e/f_0 = 0.44$.

At $f_e/f_0 = 1$, attainment of remarkably sharp, large-amplitude spectral peaks over the entire range of KC from 4 to 10 is evident. These peaks extend from the subharmonic $f/f_e = 0.5$ to $f/f_e = 3.5$.

These observations of the spectra at $f_e/f_0 = 0.44$ and 1.0 are generally in accord with those of the time signatures of § 6.1, keeping in mind that the spectra incorporate, in addition to the highly organized traces of figure 11, intermittent, less-organized segments as well. These spectra may therefore be employed to anticipate the occurrence of lock-on of both the loading and the patterns of vorticity. Spectra with sharply defined peaks are typically associated with phase-locking with, i.e. lock-on to, the cylinder motion. Furthermore, these spectra are also indicative of the degree of repetition of Lissajous trajectories, of the type shown in figures 5(*a*) and 5(*b*), for successive cycles of the cylinder motion. For example, comparison of trajectories of $C_y(t)$ versus $x_c(t)$ over a range of $4 \leqslant KC \leqslant 10$ at $f_e/f_0 = 0.44$ and 1.0 (not shown herein) reveals that the degree of congruence of a number of cycles of $C_y(t)$ versus $x_c(t)$ is strongly correlated to the degree of sharpness of the spectral peaks of figure 12.

If the frequency ratios are at, and in the vicinity of, the first harmonic of cylinder oscillation, i.e. $f_e/f_0 = 2.0$ and 2.27, the spectra exhibit broadband peaks of substantially lower amplitude. Finally, in the limiting case of zero current, represented by $U = 0$ in the top row of spectra of figure 12, sharply defined peaks occur with the predominant one consistently at $f_e/f_0 = 2.0$.

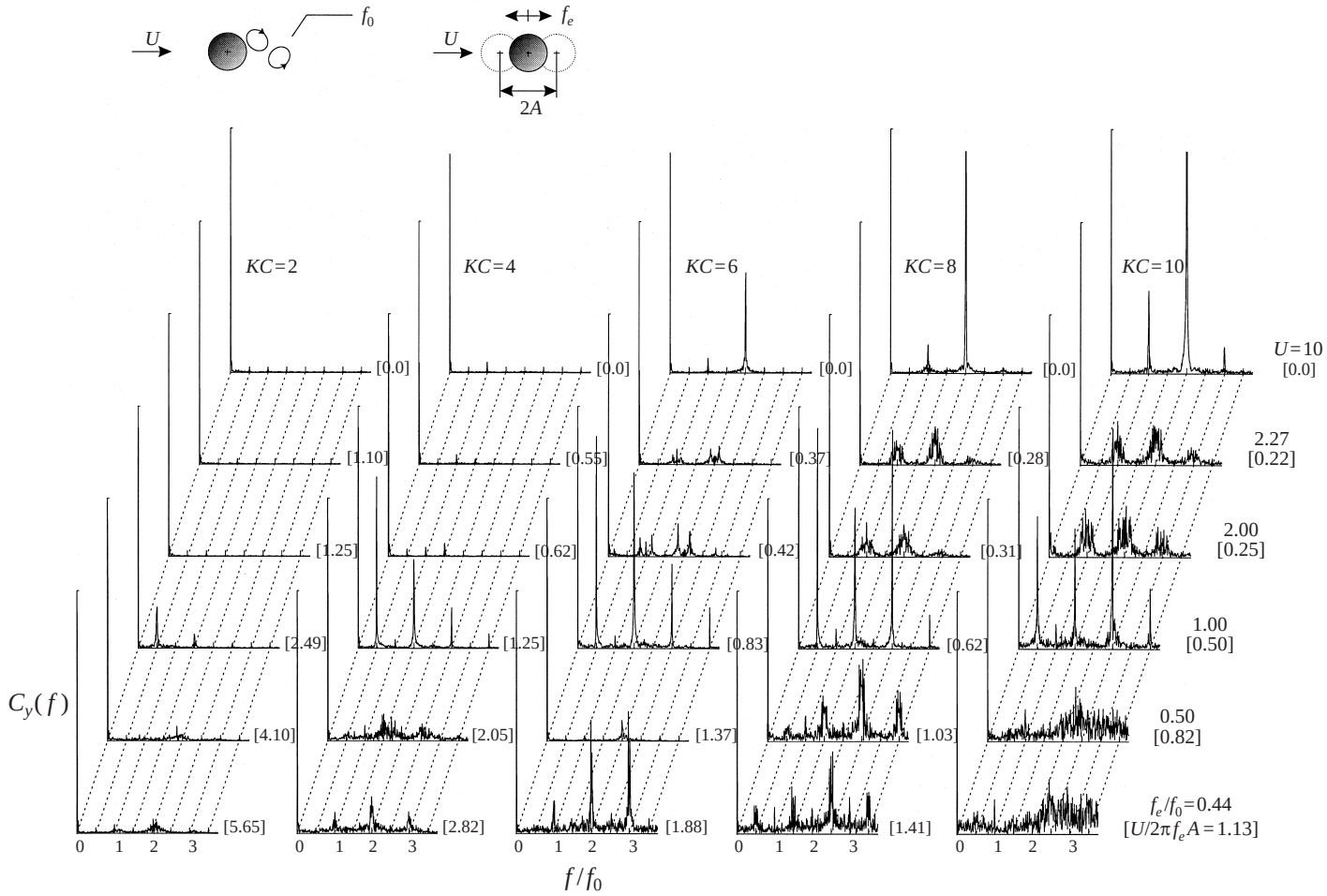

FIGURE 12. Spectra corresponding to long-time traces of $C_y(t)$, from which the excerpts of figure 11 were extracted. A total of 102 cycles of the cylinder oscillation were employed to calculate these spectra.

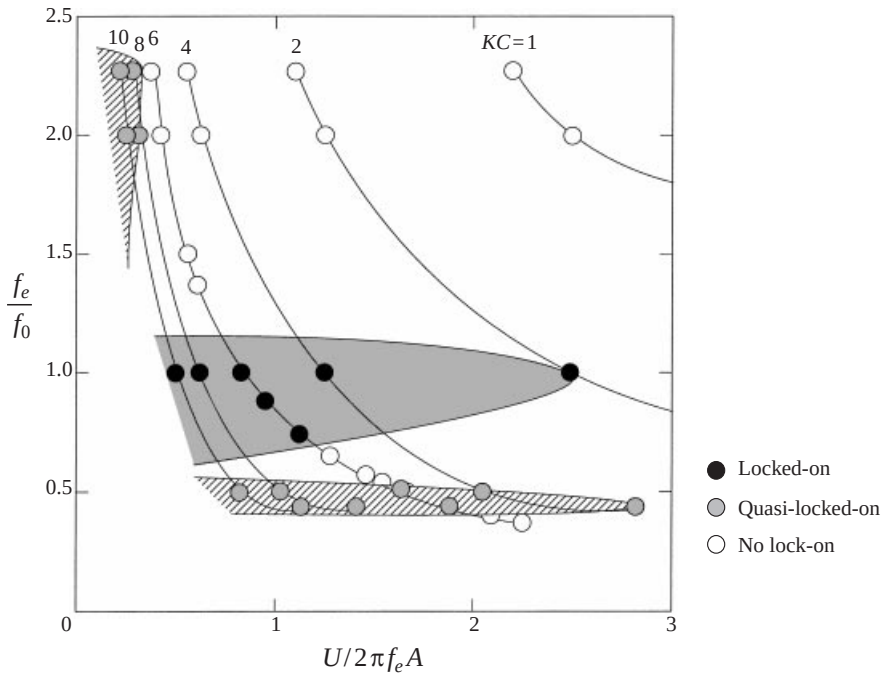

FIGURE 13. Overview of regimes of non-lock-on (hollow circular symbols), intermittent lock-on (grey-shaded circles), and locked-on (black circles) loading of the cylinder in relation to dimensionless frequency f_e/f_0 of cylinder oscillation, ratio of free-stream to cylinder velocity $U/2\pi f_e A$, and Keulegan–Carpenter number $KC = 2\pi A/D$. Degree of lock-on was determined from time traces and spectra of the transverse force coefficient C_y.

6.3. *Overview of locked-on states*

Figure 13 gives an overview of locked-on states in the plane of dimensionless excitation frequency f_e/f_0 vs. velocity ratio $U/2\pi f_e A$, with parametric variations in Keulegan–Carpenter number KC. The degree of lock-on was determined by inspection of long time traces of the transverse force coefficient C_y and the corresponding spectra. In essence, the degrees of lock-on are classified as: (i) no lock-on, either due to very low amplitude of C_y or to highly intermittent fluctuations of C_y (hollow circular symbols); (ii) intermittent lock-on, whereby locked-on, i.e. phase-locked, fluctuations of C_y relative to cylinder displacement $x_c(t)$ exist over a significant portion of the long time trace; during the remaining portions, however, the fluctuations of C_y exhibit intermittent and non-phase-locked behaviour (grey circular symbols); and (iii) locked-on oscillations of C_y where phase-locked behaviour persisted over the entire length of the record, encompassing 102 cycles of cylinder oscillation (black circular symbols).

At sufficiently large velocity ratio $U/2\pi f_e A > 3$ (not shown), only category (i), non-lock-on, occurs. At sufficiently small $U/2\pi f_e A$ and sufficiently large KC, intermittent lock-on is attainable in the vicinity of the frequency ratio $f_e/f_0 \approx 2$, corresponding to first-harmonic excitation. At $f_e/f_0 \approx 0.5$, representing approximately subharmonic excitation, category (ii), quasi-lock-on, occurs over wide ranges of $U/2\pi f_e A$ and KC. Finally, category (iii), locked-on oscillations, is also attainable over substantial ranges

of $U/2\pi f_e A$ and KC for oscillations of the cylinder at or near the fundamental frequency, $f_e/f_0 \approx 1.0$.

7. Concluding remarks

Streamwise oscillations in the presence of a steady current can give rise to fascinating types of locked-on patterns of vortex formation and, correspondingly, highly ordered modulations of the transverse force coefficient C_y. Although this type of lock-on might be viewed as analogous to that occurring for the classical case of a cylinder oscillating in the transverse direction in a uniform flow, it is distinctively different in the following respects:

(*a*) The time traces of C_y exhibit complex, ordered modulations and, correspondingly, the spectra exhibit a number of sharply defined spectral peaks. In contrast, the well-known case of transverse oscillations of the cylinder at a frequency close to, or at, the frequency of Kármán vortex formation give rise to essentially sinusoidal fluctuations of C_y and, correspondingly, a single, sharply defined peak in the spectrum.

(*b*) A frequency coalescence concept is not appropriate for the present case of in-line oscillations of the cylinder; a single, predominant frequency is never attained at lock-on. On the other hand, for the extensively studied case of the transversely oscillating cylinder, the onset of lock-on is accompanied by coalescence of two principal frequency components: the inherent, vortex formation frequency f_0 from the corresponding stationary cylinder and the externally imposed excitation frequency f_e. Regarding possible criteria for defining lock-on, a variety of approaches have been employed in previous investigations, including qualitative visualization and single-point velocity fluctuations in the wake, relative to the cylinder motion. The present approach has attempted to define lock-on by considering several representations: time histories of the transverse force C_y fluctuations; corresponding spectra of these forces; and instantaneous, global patterns of vorticity in the near wake. This approach has allowed the establishment of new types of locked-on vortex formation and loading.

In the present investigation, it is demonstrated that for sufficiently high KC and sufficiently low $U/2\pi f_e A$, intermittent and long-term lock-on are attainable for frequency ratios in the vicinity of $f_e/f_0 = 0.5$, 1.0, and 2.0. The modulations of the transverse force coefficient C_y can be directly related to the occurrence of Kármán-like vortex formation over a portion of the oscillation cycle and in a 'frozen' pattern of vorticity over the remaining portion of the cycle. The latter tends to occur over that part of the oscillation cycle where the difference in free-stream velocity U and instantaneous cylinder velocity U_c, $U - U_c$, is minimal, while Kármán-like vortex formation tends to occur when $U - U_c$ is relatively large. The signature of the transverse force coefficient $C_y(t)$ can be linked directly to the order of occurrence of patterns of Kármán-like shedding and nearly 'frozen' patterns of vorticity in the near wake. The spectra corresponding to these signatures exhibit a number of well-defined peaks. A remarkable observation is that the predominant spectral peak can undergo a six-fold change, transforming from $f/f_e = 0.5$ to 3.0 when the oscillation frequency f_e/f_0 decreases by a factor of only 2.

The loading on the cylinder has been characterized in terms of Lissajous trajectories of the transverse versus the in-line force coefficient, i.e. $C_y(t)$ versus $C_x(t)$. These complex, but ordered trajectories reflect the multiple-frequency content of quasi-phase-locked and phase-locked oscillations. Furthermore, trajectories of the transverse force coefficient $C_y(t)$ versus $x_c(t)$ show that positive hysteresis occurs over a portion of the oscillation cycle. In some cases, it is offset by an equal amount of negative hysteresis.

In other cases, the hysteresis is predominantly positive over the entire cycle. On the other hand, trajectories of the in-line force coefficient $C_x(t)$ versus displacement $x_c(t)$ exhibit only mild changes in form and the hysteresis is consistently negative over the oscillation cycle.

The central focus of the present investigation has been on identification of new types of locked-on vortex formation and their relation to time traces, Lissajous trajectories and spectra of the loading on the cylinder, as summarized in the foregoing. (The underlying concept leading to such lock-on is a delay in completion of a full cycle of Kármán-like shedding from the cylinder, and one expects the basic types of vorticity patterns observed herein to be a generic feature.) The essential features of these locked-on states and the associated loading are expected to be present over significant portions of the parameter space involving f_e/f_0, $U/2\pi f_e A$ and KC. Indeed, consideration of the form of the instantaneous and spectral representations of the force traces suggest that this is the case. Hopefully, the present investigation will serve as a basis for further studies extending over wide ranges of the aforementioned parameter space, including, in addition, the Reynolds numbers $Re = UD/\nu$ based on the steady inflow and $Re = KC(fD^2/\nu)$ based on the oscillatory conditions. The present experiments have addressed values of UD/ν lying in the range $405 \leqslant UD/\nu \leqslant 2482$. This corresponds to the so-called sensitive range, for which the vortex formation length from the corresponding stationary cylinder is relatively long, as shown by Unal & Rockwell (1988) and Lin, Towfighi & Rockwell (1995). To put matters into perspective, it should be kept in mind that a physical understanding of issues related to wide variations of $Re = UD/\nu$ for the case of classical vortex formation and loading from a transversely oscillating cylinder in a steady current in the absence of wave motion is incomplete. Similarly, the physics associated with variations of $Re = KC(fD^2/\nu)$ for oscillatory wave motion in the absence of steady current have not been adequately resolved. Each of these classes of flows represents a more restricted number of parameters than the present case, yet the physics is complex. With the use of combined quantitative imaging and simultaneous force measurements, it is hoped that the physical aspects of these classes of flow–structure interaction can be effectively addressed in the near future.

Finally, the types of phase-locked patterns of vortex formation and corresponding modulations of the force coefficient $C_y(t)$ can be described, in general, as combined frequency- and amplitude-modulated phenomena. Potential links exist between the present types of lock-on for a cylinder subjected to purely sinusoidal excitation and those arising from a cylinder subjected to amplitude- or frequency-modulated excitation in the transverse direction, as described by Nakano & Rockwell (1993, 1994). For the case of amplitude-modulated excitation, they demonstrated that several states of the near wake were attainable. They defined a locked-on wake structure, which is defined as periodic at the modulation frequency; a period-doubled wake structure, which is periodic at a frequency corresponding to half the modulation frequency; and a destabilized structure of the wake. The destabilized wake is accompanied by substantial phase modulations of the vortex formation relative to the cylinder displacement. Moreover, in the event that frequency-modulated excitation of the transversely oscillating cylinder is invoked, it is possible to either destabilize or restabilize the degree of organization of the patterns of vortices and thereby alter the spectral content of the near wake, relative to that which occurs for purely sinusoidal excitation. Such destabilization and restabilization could be attained by either varying the frequency deviation while holding the modulation frequency constant or vice-versa. Looking beyond the area of flow–structure interaction, these observations, along with those of the present study, suggest that substantial alterations in near-wake mixing may be attainable.

The authors gratefully acknowledge the Office of Naval Research for support of this investigation under Grant N00014-94-1-0185, P00007, monitored by Dr Thomas Swean. Supplemental support was provided by Office of Naval Research Grant N00014-99-1-0581, as well as by NSF Grant CTS-9803734, monitored by Dr Roger Arndt and Dr John Foss.

REFERENCES

Bearman, P. W. 1984 Vortex shedding from oscillating bluff bodies. *Ann. Rev. Fluid Mech.* **16**, 195–222.

Bearman, P. W., Downie, M. J., Graham, J. M. R. & Obasaju, E. D. 1985 Forces on cylinders in viscous oscillating flow at low Keulegan–Carpenter numbers. *J. Fluid Mech.* **154**, 337–356.

Bearman, P. W., Graham, J. M. R., Naylor, P. & Obasaju, E. D. 1981 The role of vortices in oscillatory flow about bluff cylinders. *Intl Symp. on Hydrodynamics and Ocean Engineering, the Norwegian Institute of Technology*, pp. 621–644.

Blackburn, H. M. & Henderson, R. D. 1995 Near-wake vorticity dynamics in bluff-body flows. *Proc. 12th Australasian Fluid Mechanics Conference, December, Sydney.*

Blackburn, H. & Henderson, R. 1999 A study of the two-dimensional flow past an oscillating cylinder. *J. Fluid Mech.* **385**, 255–286.

Graham, J. M. R., Arkell, R. H. & Zhou, C.-Y. 1993 The effect of combinations of mean current and oscillatory flow on the forces induced on a bluff body. *J. Wind Engng Indust. Aerodyn.* **50**, 85–96.

Griffin, O. M. & Hall, M. S. 1991 Review – vortex shedding locked-on and flow control in bluff-body wakes. *Trans. ASME*: *J. Fluids Engng* **113**, 526–537.

Griffin, O. M. & Hall, M. S. 1995 Vortex shedding lock-on in a circular cylinder wake. In *Flow-Induced Vibration* (ed. P. W. Bearman), pp. 3–14. Rotterdam/Brookfield: A. A. Balkema Press.

Griffin, O. M. & Ramberg, S. E. 1976 Vortex shedding from a cylinder vibrating in line with an incident uniform flow. *J. Fluid Mech.* **75**, 257–271.

Gu, W., Chyu, C. & Rockwell, D. 1994 Timing of vortex formation from an oscillating cylinder. *Phys. Fluids* **6**, 3677–3682.

Hall, M. S. & Griffin, O. M. 1993 Vortex shedding and lock-on in a perturbed flow. *Trans. ASME*: *J. Fluids Engng* **115**, 283–291.

Hurlburt, S. E., Spaulding, M. L. & White, F. M. 1982 Numerical solution for laminar two-dimensional flow about a cylinder oscillating in a uniform stream. *Trans. ASME*: *J. Fluids Engng* **104**, 214–222.

Ikeda, S. & Yamamoto, Y. 1981 Lift forces on cylinders in oscillatory flows. *Rep. of Department Foundation of Engineering and Coastal Engineering, Saitama University, Japan*, Vol. 10, pp. 1–16.

Iwagaki, Y., Asano, T. & Nagai, F. 1983 Hydrodynamic forces on a circular cylinder placed in wave-current co-existing fields. *Memo Faculty of Engineering, Kyoto University, Japan*, Vol. 45, pp. 11–23.

Lecointe, Y. & Piquet, J. 1989 Flow structure in the wake of an oscillating cylinder. *Trans. ASME*: *J. Fluids Engng* **111**, 139–148.

Lighthill, J. 1986 Fundamentals concerning wave loading on off-shore structures. *J. Fluid Mech.* **173**, 667–681.

Lin, X. W., Bearman, P. W. & Graham, J. M. R. 1996 A numerical study of oscillatory flow about a circular cylinder for low values of beta parameter. *J. Fluids Struct.* **10**, 501–526.

Lin, J.-C. & Rockwell, D. 1999 Horizontal oscillations of a cylinder beneath the free-surface: vortex formation and loading. *J. Fluid Mech.* **389**, 1–26.

Lin, J.-C., Towfighi, J. & Rockwell, D. 1995 Instantaneous structure of the near-wake of a circular cylinder: on the effect of Reynolds number. *J. Fluids Struct.* **9**, 409–418.

Lu, X.-Y. & Dalton, C. 1996 Calculation of the timing of vortex formation from an oscillating cylinder. *J. Fluids Struct.* **10**, 527–541.

Maull, D. J. & Milliner, M. C. 1978 Sinusoidal flow past a circular cylinder. *Coastal Engng* **2**, 149–168.

Nakano, M. & Rockwell, D. 1993 The wake from a cylinder subjected to amplitude-modulated excitation. *J. Fluid Mech.* **247**, 79–110.

Nakano, M. & Rockwell, D. 1994 Flow structure in the frequency-modulated wake of a cylinder. *J. Fluid Mech.* **266**, 93–119.

Obasaju, E. D., Bearman, P. W. & Graham, J. M. R. 1988 A study of forces, circulation, vortex patterns around a circular cylinder in oscillating flow. *J. Fluid Mech.* **196**, 467–494.

Öngoeren, A. & Rockwell, D. 1988 Flow structure from an oscillating cylinder. Part 2. Mode competition in the near-wake. *J. Fluid Mech.* **197**, 225–246.

Rockwell, D. 1990 Active control of globally-unstable separated flows. *Intl Symp. on Unsteady Flow Dynamics* (ed. J. A. Miller & D. P. Telionis). ASME, FED-92.

Rockwell, D., Magness, C., Towfighi, J., Akin, O. & Corcoran, T. 1993 High-image-density particle image velocimetry using laser scanning techniques. *Exps Fluids* **14**, 181–192.

Sarpkaya, T. 1979 Vortex induced oscillations: a selective review. *Trans. ASME*: *J. Appl. Mech.* **46**, 241–258.

Sarpkaya, T. 1989 Computation methods with vortices – the 1988 Freeman Scholar Lecture. *Trans. ASME*: *J. Fluids Engng* **111**, 5–52.

Sarpkaya, T., Bakinis, C. & Storm, M. A. 1984 Hydrodynamic forces from combined wave and current flow on smooth and rough circular cylinders at high Reynolds numbers. *Ocean Technology Conference, Houston, TX, October*, p. 4830.

Sarpkaya, T. & Isaacson, M. 1981 *Mechanics of Wave Forces on Offshore Structures*. Van Nostrand Reinhold.

Sarpkaya, T., Putzig, C., Gordon, D., Wang, X. & Dalton, C. 1992 Vortex trajectories around a circular cylinder in oscillatory plus mean flow. *Trans. ASME*: *J. Offshore Mech. Arctic Engng* **114**, 291–298.

Sarpkaya, T. & Storm, M. 1985 In-line force on a cylinder translating in an oscillatory flow. *Appl. Ocean Res.* **7**, 188–196.

Sheridan, J., Carberry, J., Lin, J.-C. & Rockwell, D. 1998 On the near-wake topology of an oscillating cylinder. *J. Fluids Struct.* **12**, 215–220.

Singh, S. 1979 Forces on bodies in oscillatory flow. PhD thesis, University of London.

Tanida, Y., Okajima, A. & Watanabe, Y. 1973 Stability of a circular cylinder oscillating in uniform flow or in a wake. *J. Fluid Mech.* **61**, 769–784.

Unal, F. & Rockwell, D. 1988 Vortex formation from a cylinder. Part 1. The initial instability. *J. Fluid Mech.* **190**, 491–512.

Verley, R. L. P. & Moe, G. 1979 The forces on a cylinder in oscillating current. *The Norwegian Institute of Technology*, STF60 A79061 (25 Flow Visualization Film Prints).

Williamson, C. H. K. 1985 Sinusoidal flow relative to circular cylinder. *J. Fluid Mech.* **155**, 141–174.

Williamson, C. H. K. & Roshko, A. 1988 Vortex formation in the wake of an oscillating cylinder. *J. Fluids Struct.* **2**, 355–381.

Zdravkovich, M. M. 1982 Modification of vortex shedding in the synchronization range. *Trans. ASME*: *J. Fluids Engng* **104**, 513–517.

Zdravkovich, M. M. 1996 Inadequacy of a conventional Keulegan–Carpenter number for wave and current combination. *J. Offshore Mech. Arctic Engng* **118**, 309–311.